

# Computational imaging systems: joint design and end-to-end optimality

Tejaswini Mirani,<sup>1,\*</sup> Dinesh Rajan,<sup>1</sup> Marc P. Christensen,<sup>1</sup> Scott C. Douglas,<sup>1</sup>  
and Sally L. Wood<sup>2</sup>

<sup>1</sup>Department of Electrical Engineering, Southern Methodist University, 6251 Airline Road, Dallas, Texas 75275-0338, USA

<sup>2</sup>Department of Electrical Engineering, Santa Clara University, 500 El Camino Real, Santa Clara, California 95053-1500, USA

\*Corresponding author: tmirani@engr.smu.edu

Received 11 September 2007; revised 10 January 2008; accepted 25 January 2008;  
posted 5 February 2008 (Doc. ID 87361); published 0 MONTH 0000

A framework is proposed for optimal joint design of the optical and reconstruction filters in a computational imaging system. First, a technique for the design of a physically unconstrained system is proposed whose performance serves as a universal bound on any realistic computational imaging system. Increasing levels of constraints are then imposed to emulate a physically realizable optical filter. The proposed design employs a generalized Benders' decomposition method to yield multiple globally optimal solutions to the nonconvex optimization problem. Structured, closed-form solutions for the design of observation and reconstruction filters, in terms of the system input and noise autocorrelation matrices, are presented. Numerical comparison with a state-of-the-art optical systems shows the advantage of joint optimization and concurrent design. © 2008 Optical Society of America

*OCIS codes:* 110.1758, 110.3010.

## 1. Introduction

Traditionally, the entire task of image formation lies solely in the physical optics of the imaging system. Conventional imaging systems utilize a lens or mirror in the front end to form an image that is then sampled onto a detector [1]. The electronic signal processing is considered to be postprocessing that attempts to ameliorate the loss inherent in the image formation task. With the recent advances in the field of electronics, there has been a tremendous improvement in the performance of sensor electronics and display devices. As per Moore's law, the sensor electronics and display devices have better performance and a smaller form factor (size). On the other hand, the optical imagers (sensor optics) still remain bulky due to the physics of image formation, which is governed by Maxwell's equations. These comparatively slower advances made in the field of imaging systems as compared with electronics can be attributed

totraditional design approaches wherein the optical subsystem design is carried out separately from the corresponding signal processing algorithms [2]. To overcome this limitation, it is necessary to change the typical notion of an imaging system as an optical front-end followed by a detector and postdetection digital signal processing, i.e., the processes of image formation and detection can no longer be considered separable [3].

The term "computational imaging" describes the emerging field of optical systems in which a true image is not formed by a lens and simply sampled onto a detector. Rather, the process of image formation is shared between the power of the optical elements and signal processing of the sampled amplitudes. Such an imaging system integrally incorporates optics, optoelectronics, and signal processing. System performance in computational imaging systems is optimized through concurrent design and joint optimization of all elements. Several point solutions serve to illustrate the utility of this approach, as it can attain system-level performance

far exceeding separately optimized optical and reconstruction designs [3,4].

Applications of computational imaging systems include conventional imaging to produce visually pleasing images, special purpose imaging whose output is also an image but with enhanced characteristics, and functional imaging to produce information about a scene from optical data [2]. Recent advances in the field of optics have seen the trend in which the task of image formation is distributed between the optical elements and the signal processing algorithms. It has been shown that the overall imaging performance of optical sensors can be enhanced by the modification of incoming light waves (predetection filtering) in tandem with electronic signal processing (postdetection filtering) [5]. The concept and experimental verification of a computational imaging system called TOMBO, which draws inspiration from nature's design of the compound eyes of arthropods, has been presented [4,6]. TOMBO uses multiplex imaging sensors that also rely on the joint functioning of optics and electronics to obtain visual information. Another example of a successful computational imaging system is the wavefront coding system, which creates optical sensors that are capable of operating over extended depths of field [7]. Once again, the concept behind these wavefront coding imagers is the concurrent design and joint optimization of optical and signal processing systems. More specifically, the proposed design methods presented in this paper are being considered for the design of a pervasive flat form factor imaging system (PANOPTES), i.e., a flat optical sensor that contains a multitude of low-resolution micro-optical sensors [8–10]. A thin optical sensor would be restricted to using smaller optical elements and therefore require additional computation to augment the image formation to achieve high resolution, which again implies that joint design of optical sensors and signal processing elements is required.

This paper presents a design framework for the joint design of optical and reconstruction filters in a computational imaging system. We consider the joint optimization of the optics and the signal processing to achieve end-to-end optimality. We use the mean squared error (MSE) between the reconstructed image and the original scene as the performance metric to optimize. Initially, a universal bound on the performance of computational imaging systems is derived. Although this bound is derived without any physical constraints on the optical elements, it provides insights into the structure of optical filters. The goal of studying unconstrained optimization is to find a theoretically ideal system manifesting the maximum benefits that can be attained, if the ability to build such a system existed. To make the transition from this theoretically ideal system to a physically realizable one, a series of constraints are imposed on the optical system. The types of constraints that we consider include energy conservation of the optical system (photons only

detected once), isoplanatism of the optical field (rows of the observation matrix are shifted versions of each other), and low-pass response of the optical system (corresponding to the limiting physical aperture). Closed-form solutions to the design of an unconstrained optical system are provided. A numerically optimized energy-conserving optical system is presented. Large signal-to-noise (SNR) approximations are made to obtain closed-form solutions for energy-conserving optical systems. We show that a multitude of solutions exist for the globally optimal observation and reconstruction filters. The proposed optimal filters are then compared with state-of-the-art optical systems to quantify their performance and potential margin for improvement.

The proposed design yields globally optimal observation and reconstruction filters, even though the optimization problem is nonconvex. The globally optimal solution for the nonconvex optimization problem is obtained by using a generalization of Benders' decomposition [11]. Specifically, we leverage the structure of the nonconvex problem to partition the problem into two easily tractable optimization problems. The design of the optimal observation and reconstruction matrices also uses tools from convex optimization [12,13], principal component analysis [14], and linear algebra [15,16]. The proposed construction technique depends on the statistics of the signal and noise and applies equally to the case of white and colored noise models.

The paper is organized as follows: The system model, along with the problem definition, is given in Section 2. The unconstrained optimization problem is solved in Section 3. In Section 4, numerical as well as analytical solutions in the high SNR regime to the energy-conserving optimization problem are presented. In Sections 5 and 6, we quantify the performance of commonly used optical systems and contrast them with the proposed optimal filters. The conclusions are presented in Section 7.

## 2. Computational Imaging System

### A. System Model

The block diagram detailing the imaging system of interest is shown in Fig. 1. We use small boldface letters for vectors and capital boldface for matrices. A two-dimensional scene of interest of size  $k_x \times k_y$  is represented by a column vector, denoted  $\mathbf{f}$ , of size  $n \times 1$ , where  $n = k_x k_y$ . It is assumed that the input scene is sampled at the highest resolution of interest. The optical system consisting of the lens along with the effect of the detector is modeled by the observation matrix  $\mathbf{H}$  of dimensions  $m \times n$ . The main case of interest to us is when the number of pixels at the detector is less than the number of pixels in the original scene at the highest resolution of the imager, i.e.,  $m \leq n$ . The output,  $\mathbf{g}$ , of the observation filter at the detector array is given by

$$\mathbf{g} = \mathbf{H}\mathbf{f} + \mathbf{z}, \quad (1)$$

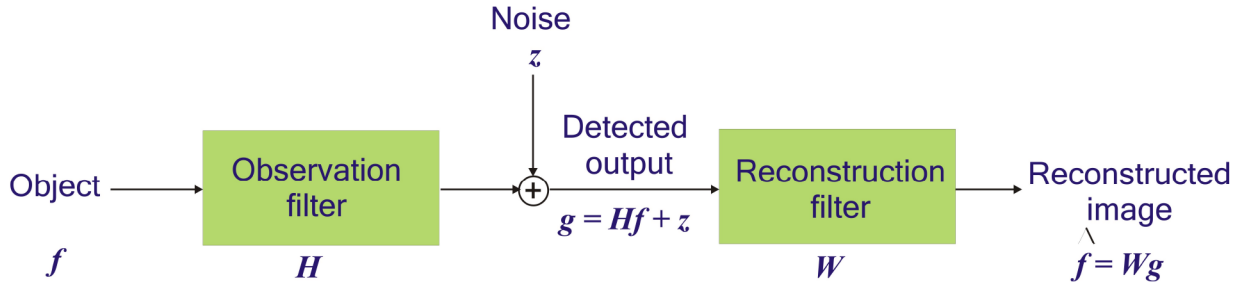


Fig. 1. (Color online) Simplified block diagram.

where  $\mathbf{z}$  represents the effective measurement noise in the system and is assumed to be a Gaussian random variable with mean zero and autocorrelation  $\mathbf{R}_z$ . The noise vector  $\mathbf{z}$  and the detected output vector  $\mathbf{g}$  are of dimensions  $m \times 1$ . We denote by matrix  $\mathbf{W}$  the effect of the reconstruction filter. The dimensions of  $\mathbf{W}$  are  $n \times m$ , and the reconstruction filter linearly processes the detected output  $\mathbf{g}$ . The output of the reconstruction process  $\mathbf{W}$  is the reconstructed signal  $\hat{\mathbf{f}}$ , given by

$$\hat{\mathbf{f}} = \mathbf{W}\mathbf{g} = \mathbf{W}(\mathbf{H}\mathbf{f} + \mathbf{z}). \quad (2)$$

Traditional image processing systems aim to optimize a chosen metric (e.g., MSE), by designing the reconstruction matrix  $\mathbf{W}$  [17]. The optics in these traditional systems, represented by observation matrix  $\mathbf{H}$ , is considered to be constant (fixed): the objective is to design the lens so that a sharp image is obtained at the detector or the detected image has a SNR. The reconstruction matrix  $\mathbf{W}$  in such a system is considered to be the postprocessor that rectifies the aberrations (imperfections) caused by the lens. In contrast, the goal of the proposed computational imaging system is to attain end-to-end optimality by jointly designing the observation matrix  $\mathbf{H}$  and the reconstruction matrix  $\mathbf{W}$ . Selecting the standard MSE metric for the end-to-end optimization, we formally set up the optimization problem in the next section.

#### B. Performance Metric: End-to-End MSE

The end-to-end error associated with the image formation task is given by

$$\mathbf{e} = \mathbf{f} - \hat{\mathbf{f}}. \quad (3)$$

The MSE,  $J$ , can then be computed as

$$J = \mathbb{E}[\mathbf{e}^t \mathbf{e}] = \mathbb{E}[\text{Tr}(\mathbf{e}\mathbf{e}^t)],$$

where  $\text{Tr}[\mathbf{A}]$  is the trace of  $\mathbf{A}$ , superscript  $t$  refers to matrix transpose, and  $\mathbb{E}$  denotes the expectation operator. This MSE can be further simplified as

$$\begin{aligned} J &= \mathbb{E}[\text{Tr}(\mathbf{e}\mathbf{e}^t)] = \mathbb{E}[\text{Tr}[(\mathbf{f} - \mathbf{W}\mathbf{g})(\mathbf{f} - \mathbf{W}\mathbf{g})^t]] \\ &= \mathbb{E}[\text{Tr}[\mathbf{f}\mathbf{f}^t - \mathbf{W}(\mathbf{H}\mathbf{f}\mathbf{f}^t + \mathbf{z}\mathbf{f}^t) - (\mathbf{f}\mathbf{f}^t\mathbf{H}^t + \mathbf{f}\mathbf{z}^t)\mathbf{W}^t \\ &\quad + \mathbf{W}(\mathbf{H}\mathbf{f}\mathbf{f}^t\mathbf{H}^t + \mathbf{z}\mathbf{f}^t\mathbf{H}^t + \mathbf{H}\mathbf{f}\mathbf{z}^t + \mathbf{z}\mathbf{z}^t)\mathbf{W}^t]]. \end{aligned} \quad (4)$$

We assume that the noise has zero mean and that there is no correlation between the noise and the image data so that  $\mathbb{E}[\mathbf{f}\mathbf{z}^t] = \mathbb{E}[\mathbf{z}\mathbf{f}^t] = 0$ . Also, since the trace is linear, the trace and the expectation operators commute. Hence, the MSE can be simplified as

$$\begin{aligned} J &= \text{Tr}\{\mathbb{E}[\mathbf{f}\mathbf{f}^t] - \mathbb{E}[\mathbf{W}\mathbf{H}\mathbf{f}\mathbf{f}^t] - \mathbb{E}[\mathbf{f}\mathbf{f}^t\mathbf{H}^t\mathbf{W}^t] \\ &\quad + \mathbb{E}[\mathbf{W}\mathbf{H}\mathbf{f}\mathbf{f}^t\mathbf{H}^t\mathbf{W}^t] + \mathbb{E}[\mathbf{W}\mathbf{z}\mathbf{z}^t\mathbf{W}^t]\}. \end{aligned} \quad (5)$$

Define the autocorrelation of the signal  $\mathbf{R}_f$  and the autocorrelation of noise  $\mathbf{R}_z$  as

$$\mathbf{R}_f = \mathbb{E}[\mathbf{f}\mathbf{f}^t], \quad \mathbf{R}_z = \mathbb{E}[\mathbf{z}\mathbf{z}^t]. \quad (6)$$

Simplifying Eqs. (5) by using Eq. (6), the MSE,  $J$ , which is a function of  $\mathbf{H}$  and  $\mathbf{W}$ , is given by

$$\begin{aligned} J &= \phi(\mathbf{H}, \mathbf{W}) \\ &= \text{Tr}[\mathbf{R}_f - 2\mathbf{W}\mathbf{H}\mathbf{R}_f + \mathbf{W}\mathbf{H}\mathbf{R}_f\mathbf{H}^t\mathbf{W}^t + \mathbf{W}\mathbf{R}_z\mathbf{W}^t]. \end{aligned} \quad (7)$$

In the next subsection, we describe the variables of optimization and the constraints that are imposed on the optimization problem.

#### C. Optimization Framework

As mentioned before, in traditional imaging systems only the reconstruction matrix  $\mathbf{W}$  is optimized to minimize the MSE. The optimal reconstruction matrix  $\mathbf{W}^*$  for a fixed observation matrix  $\mathbf{H}$  is given by the following well-known Wiener filter [17,18]:

$$\mathbf{W}^* = \mathbf{R}_f\mathbf{H}^t(\mathbf{H}\mathbf{R}_f\mathbf{H}^t + \mathbf{R}_z)^{-1}. \quad (8)$$

As opposed to traditional imaging systems, we optimize jointly over the reconstruction and observation filters to attain system level optimality. Initially, no constraints are imposed on the system to study the properties of the optimal filters that yield the lowest possible MSE. The joint optimization problem over the two variables  $\mathbf{H}$  and  $\mathbf{W}$  with no constraints is defined next.

## 1. Unconstrained Optimization

The unconstrained joint optimization problem over  $\mathbf{H}$  and  $\mathbf{W}$  is posed as

$$\min_{\{\mathbf{H}, \mathbf{W}\}} \text{Tr}[\mathbf{R}_f - 2\mathbf{W}\mathbf{H}\mathbf{R}_f + \mathbf{W}\mathbf{H}\mathbf{R}_f\mathbf{H}^t\mathbf{W}^t + \mathbf{W}\mathbf{R}_z\mathbf{W}^t]. \quad (9)$$

In Eq. (9) no constraints have been imposed on the domain of  $\mathbf{H}$  and  $\mathbf{W}$ , i.e.,  $\mathbf{H} \in \mathbb{R}^{m \times n}$  and  $\mathbf{W} \in \mathbb{R}^{n \times m}$ , where  $m < n$  for the imaging system of interest. Clearly, solutions to this unconstrained problem may not lead to physically realizable optical lenses and detectors. However, the solution of problem (9) serves as a lower bound on the MSE of all practically realizable systems.

It can be easily shown that the objective function in Eq. (9) is convex in  $\mathbf{H}$  with  $\mathbf{W}$  fixed and convex in  $\mathbf{W}$  with  $\mathbf{H}$  fixed. However, the problem is not jointly convex in  $\mathbf{H}$  and  $\mathbf{W}$ . (The Hessian of  $J$  computed over  $\mathbf{H}$  and  $\mathbf{W}$  is not positive definite, i.e.,

$$D = \begin{bmatrix} \frac{\partial^2 J}{\partial H^2} & \frac{\partial^2 J}{\partial H \partial W} \\ \frac{\partial^2 J}{\partial W \partial H} & \frac{\partial^2 J}{\partial W^2} \end{bmatrix}$$

is not positive definite.) In Section 3, we solve this nonconvex problem in closed form and suggest a procedure for the design of the globally optimal observation matrix  $\mathbf{H}^*$  and reconstruction matrix  $\mathbf{W}^*$ .

## 2. Optimization with Physical Constraints

Recall, that the observation filter denotes the combined effect of the optical lens and the detector. The laws of physics governing the functioning of the lens and detector impose certain constraints on the observation matrix  $\mathbf{H}$ , such as

1. Rows of  $\mathbf{H}$  sum to one.
2. All elements of  $\mathbf{H}$  are nonnegative.
3. Physically realizable observation filters.

The first two constraints correspond to the fact that the photons in the optical system can be sensed only once. In addition to photons being sensed once, we also consider certain properties that make physically realizable optical filters commonly used in practice such as isoplanatism of the optical field and low-pass response of the optical system. We approach these physically significant constraints in sequence, thereby allowing us to examine the implications of each.

- Constraint 1: Energy conservation (rows of  $\mathbf{H}$  sum to one)

Clearly, the number of photons detected in the system cannot exceed the number of photons emitted by the source. In the formation of an optical image, each surface of the object gives rise to a blurred distribution in the image surface of total brightness proportional to that of the object element. Since we consider

the object elements to be incoherently lit, the intensities add up to give us the distribution of the image. To ensure that photons are sensed only once implies that the sum of each row of the observation matrix is equal to 1. If the sum is less than one, then some photons are not collected by the system, leading to suboptimum performance. To achieve a sum greater than one would require optical “gain” in the sensing system, i.e., the amount of light collected from a single object point exceeds the amount present. The computational imaging system of interest is a passive one, and it is not possible to obtain gain of optical energy in a passive system. Hence, it is required that the sum of all rows in the observation matrix be equal to unity. We denote by  $\mathbf{H}_{ec}$  an observation matrix with the property that the rows sum to one. The corresponding reconstruction matrix is denoted by  $\mathbf{W}_{ec}$ . The constraint set  $\mathcal{H}_{ec}$  is defined as

$$\mathcal{H}_{ec} = \{\mathbf{H}_{ec} : \mathbf{H}_{ec}\mathbf{j}_{n \times 1} = \mathbf{j}_{m \times 1}\}, \quad (10)$$

where  $\mathbf{j}_{a \times b}$  is a matrix of size  $a \times b$  with all elements being equal to unity. It is straightforward to verify that the set  $\mathcal{H}_{ec}$  is a convex set. We now define the new constrained optimization problem as

$$\begin{aligned} \min_{\{\mathbf{H}_{ec} \in \mathcal{H}_{ec}, \mathbf{W}_{ec}\}} J_{ec} = & \text{Tr}[\mathbf{R}_f - 2\mathbf{W}_{ec}\mathbf{H}_{ec}\mathbf{R}_f \\ & + \mathbf{W}_{ec}\mathbf{H}_{ec}\mathbf{R}_f\mathbf{H}_{ec}^t\mathbf{W}_{ec}^t + \mathbf{W}_{ec}\mathbf{R}_z\mathbf{W}_{ec}^t], \end{aligned} \quad (11)$$

where the subscript *ec* refers to energy conservation optimization. We provide an analytical solution to Eq. (11) that is valid for high SNR and also suggest a procedure to design the optimal observation matrix  $\mathbf{H}_{ec}^*$  and reconstruction matrix  $\mathbf{W}_{ec}^*$ . We also construct an iterative numerical procedure to compute the optimal  $\mathbf{H}_{ec}^*$  and  $\mathbf{W}_{ec}^*$  for arbitrary SNR.

- Constraint 2: Nonnegativity (Each element of  $\mathbf{H}$  is nonnegative)

To ensure that the photons in the optical system are sensed only once, in addition to rows of the observation matrix summing to one, we need to ensure that each element of the matrix is nonnegative. Since the imaging system of interest is incoherently lit, it cannot represent negative elements [19]. Hence, we impose an additional constraint on the optimization problem, namely, each element of the observation matrix should be nonnegative. Let  $\mathbf{H}_{nneg}$  denote an observation matrix that has all its elements greater than or equal to zero. The constraint set  $\mathcal{H}_{nneg}$  is defined as

$$\mathcal{H}_{nneg} = \{\mathbf{H}_{nneg} : H_{nneg_{ij}} \geq 0 \quad \forall i = 1 \dots m, j = 1 \dots n\}, \quad (12)$$

where  $H_{nneg_{ij}}$  is the  $i$ th row,  $j$ th column element of  $\mathbf{H}_{nneg}$ .

Clearly, constraint set  $\mathcal{H}_{nneg}$  is convex, and consequently the intersection of  $\mathcal{H}_{ec}$  and  $\mathcal{H}_{nneg}$  is also



convex. We denote by  $\mathbf{H}_{\text{nec}}$  the observation matrix that is defined over the intersection of sets  $\mathcal{H}_{\text{ec}}$  and  $\mathcal{H}_{\text{nneg}}$ . The corresponding reconstruction matrix is  $\mathbf{W}_{\text{nec}}$ . The optimization problem is defined as

$$\min_{\{\mathbf{H} \in \mathcal{H}_{\text{ec}} \cap \mathcal{H}_{\text{nneg}}, \mathbf{W}_{\text{nec}}\}} \text{Tr}[\mathbf{R}_f - 2\mathbf{W}_{\text{nec}}\mathbf{H}_{\text{nec}}\mathbf{R}_f + \mathbf{W}_{\text{nec}}\mathbf{H}_{\text{nec}}\mathbf{R}_f\mathbf{H}_{\text{nec}}^t\mathbf{W}_{\text{nec}}^t + \mathbf{W}_{\text{nec}}\mathbf{R}_z\mathbf{W}_{\text{nec}}^t]. \quad (13)$$

Solving Eq. (13) analytically is difficult due to the presence of a large number of inequality constraints. An observation filter  $\mathbf{H}_{\text{nec}}$  that has its rows summing to one and all its elements greater than zero is found using numerical optimization. It turns out that there is a marginal reduction in performance with respect to the energy-conserving  $\mathbf{H}_{\text{ec}}$  due to the numerically optimized observation filter.

- **Constraint 3:** In addition to the constraints described above, we also focus our attention on the structure of a physically realizable observation matrix  $\mathbf{H}$ . Constraints on the structure of  $\mathbf{H}$  that make it physically realizable are isoplanatism of the optical field (rows of the observation matrix are shifted versions of each other) and low-pass response of the optical system (which corresponds to the limiting physical aperture). These constraint sets are nonconvex, and the optimization problems associated with these sets are very difficult to solve in closed form. To study the properties of these observation matrices with structure, we construct an observation matrix  $\mathbf{H}$  based on existing physically realizable systems that satisfy these criteria and then compare their performance with the proposed jointly optimized design.

Having formulated the various optimization problems, in the next section, we simplify and solve these optimization problems.

#### D. Problem Simplification—Partitioning of the Nonconvex Problem

The optimization problems described in Subsection 2.C are nonconvex, and hence it is challenging to find the globally optimal solution by standard methods. We solve these problems by partitioning them into two separate problems, namely inner and outer minimization, by employing the following theorem [11], which renders these problems tractable. The theorem helps us to view the problem in  $W$ -space instead of the  $HW$ -space. To better understand the theorem, we first present some definitions and explain the notation. The problem formulation is restated as

$$\min_{\{\mathbf{H}, \mathbf{W}\}} \phi(\mathbf{H}, \mathbf{W}) \quad \text{subject to} \quad \Psi(\mathbf{H}, \mathbf{W}) \geq 0, \quad (14)$$

$$\mathbf{H} \in \mathcal{H}, \mathbf{W} \in \mathcal{W}$$

where the function  $\Psi$  represents a joint constraint on  $\mathbf{H}$  and  $\mathbf{W}$ . The matrix  $\mathbf{W}$  is referred to as the

“complicating variable” in the sense that Eq. (14) is a much easier optimization problem in  $\mathbf{H}$  when  $\mathbf{W}$  is temporarily held fixed. The key idea that enables Eq. (14) to be viewed in  $W$ -space is the concept

of projection [20], sometimes referred to as “partitioning.” The projection of Eq. (14) onto  $\mathbf{W}$  is

$$\min_{\mathbf{W}} v(\mathbf{W}) \quad \text{subject to} \quad \mathbf{W} \in \mathcal{W} \cap \mathcal{V}, \quad (15)$$

where

$$v(\mathbf{W}) \equiv \inf_{\mathbf{H}} \phi(\mathbf{H}, \mathbf{W}) \quad \text{subject to} \quad \Psi(\mathbf{H}, \mathbf{W}) \geq 0, \quad (16)$$

$$\mathbf{H} \in \mathcal{H}$$

$$\mathcal{V} = \{\mathbf{W}: \Psi(\mathbf{H}, \mathbf{W}) \geq 0 \quad \text{for some} \quad \mathbf{H} \in \mathcal{H}\}. \quad (17)$$

Note that  $v(\mathbf{W})$  is the optimal value of Eq. (14) for fixed  $\mathbf{W}$  and that, by our designation of  $\mathbf{W}$  as complicating variable, evaluating  $v(\mathbf{W})$  is much easier than solving Eq. (14). The following theorem shows that an optimal solution  $\mathbf{W}^*$  of Eq. (15) also yields an optimal solution  $(\mathbf{H}^*, \mathbf{W}^*)$  of Eq. (14), where  $\mathbf{H}^*$  is the optimizing  $\mathbf{H}$  in Eq. (16).

**Theorem 2.1. (Projection)** [11] *If  $(\mathbf{H}^*, \mathbf{W}^*)$  is optimal in Eq. (14), then  $\mathbf{W}^*$  must be optimal in Eq. (15). If  $\mathbf{W}^*$  is optimal in Eq. (15) and  $\mathbf{H}^*$  achieves the infimum in Eq. (16) with  $\mathbf{W} = \mathbf{W}^*$ , then  $(\mathbf{H}^*, \mathbf{W}^*)$  is optimal in Eq. (14).*

The first statement in the theorem is fairly straightforward and is not directly applicable to our problem. We make use of the second statement in the theorem, which states that globally optimal  $(\mathbf{H}^*, \mathbf{W}^*)$  can be obtained by solving Eqs. (15) and (16). Moreover, since we do not impose any joint constraint on  $\mathbf{H}$  and  $\mathbf{W}$ , the set  $\mathcal{V}$  in Eq. (15) becomes redundant. The important point to be emphasized is that Theorem 2.1 does not require an assumption of joint convexity on Eq. (14), but it does make use of the fact that Eq. (14) is convex in  $\mathbf{H}$  with  $\mathbf{W}$  fixed and vice-versa. We designate Eq. (16) as the inner minimization problem and Eq. (15) as the outer minimization problem. Thus Theorem 2.1 enables us to split Eq. (14) into an inner Eq. (16) and an outer optimization problem (15) that when solved sequentially lead to the globally optimal solution. Note that we select  $\mathbf{W}$  as the complicating variable and perform the inner minimization over  $\mathbf{H}$  just to ease the calculation complexity. The theorem allows the optimization over the two variables to be performed in any order. In the next section, we solve the unconstrained optimization problem by using Theorem 2.1.

### 3. Unconstrained Minimization

The unconstrained minimization problem described in Eq. (9) is partitioned into inner and outer minimization problems to obtain the globally optimal solution.

#### A. Inner Minimization for Unconstrained $\mathbf{H}$

The inner minimization problem stated in Eq. (16) can be solved by the method of Lagrange multipliers for the unconstrained case.

**Proposition 1.** *For given signal and noise autocorrelations  $\mathbf{R}_f$  and  $\mathbf{R}_z$ , and a fixed reconstruction filter  $\mathbf{W}$ , the observation filter  $\mathbf{H}^*$ , without any constraints on  $\mathbf{H}$ , that minimizes the end-to-end MSE is the pseudo-inverse of the reconstruction filter  $\mathbf{W}$ , i.e.,  $\mathbf{H}^* = (\mathbf{W}^t \mathbf{W})^{-1} \mathbf{W}^t$ .*

*Proof.* The proof is immediate by applying standard Lagrangian optimization. Recall from Eq. (9), the optimization problem is

$$\min_{\{\mathbf{H}\}} J = \text{Tr}[\mathbf{R}_f - 2\mathbf{W}\mathbf{H}\mathbf{R}_f + \mathbf{W}\mathbf{H}\mathbf{R}_f\mathbf{H}^t\mathbf{W}^t + \mathbf{W}\mathbf{R}_z\mathbf{W}^t]. \quad (18)$$

Differentiating Eq. (18) with respect to  $\mathbf{H}$  and setting the gradient equal to zero, we obtain

$$\frac{\partial J}{\partial \mathbf{H}} = -2\mathbf{W}^t\mathbf{R}_f + 2\mathbf{W}^t\mathbf{W}\mathbf{H}\mathbf{R}_f = 0. \quad (19)$$

Since  $\mathbf{R}_f$  is full rank,

$$\mathbf{H}^* = (\mathbf{W}^t\mathbf{W})^{-1}\mathbf{W}^t. \quad (20)$$

□

#### B. Outer Minimization for Unconstrained $\mathbf{H}$

Having solved the inner minimization problem, we now substitute the solution of the inner problem  $\mathbf{H}^*$  from Eq. (20) into Eq. (15) to obtain the outer minimization problem. We then optimize over  $\mathbf{W}$  to obtain the globally optimal  $(\mathbf{H}^*, \mathbf{W}^*)$  in the unconstrained case. Substituting Eq. (20) into Eq. (15), we obtain the following optimization problem:

$$\min_{\{\mathbf{W}\}} \text{Tr}[\mathbf{R}_f - \mathbf{W}(\mathbf{W}^t\mathbf{W})^{-1}\mathbf{W}^t\mathbf{R}_f + \mathbf{W}\mathbf{R}_z\mathbf{W}^t]. \quad (21)$$

Differentiating (21) with respect to  $\mathbf{W}$  and setting it to zero, we obtain

$$\mathbf{W} = \mathbf{R}_f\mathbf{W}(\mathbf{W}^t\mathbf{W})^{-1}[\mathbf{R}_z + (\mathbf{W}^t\mathbf{W})^{-1}\mathbf{W}^t\mathbf{R}_f\mathbf{W}(\mathbf{W}^t\mathbf{W})^{-1}]^{-1}. \quad (22)$$

It is challenging to directly solve for  $\mathbf{W}$  in terms of  $\mathbf{R}_f$  and  $\mathbf{R}_z$  from Eq. (22). But recognize that Eq. (22) is of the form

$$\mathbf{W}^* = \mathbf{R}_f\mathbf{H}^{*t}(\mathbf{H}^*\mathbf{R}_f\mathbf{H}^{*t} + \mathbf{R}_z)^{-1}, \quad (23)$$

where

$$\mathbf{H}^* = (\mathbf{W}^{*t}\mathbf{W}^*)^{-1}\mathbf{W}^{*t} \quad (24)$$

is the solution to the inner minimization problem. Recall that the objective of the outer minimization is to find the optimal reconstruction matrix  $\mathbf{W}^*$  that satisfies Eq. (22). We achieve this objective by solving Eqs. (23) and (24) jointly to obtain  $\mathbf{H}^*$  and  $\mathbf{W}^*$ , which in turn satisfies Eq. (22). Substitute Eq. (23) into Eq. (24) to obtain

$$\begin{aligned} \mathbf{H} &= ((\mathbf{R}_f\mathbf{H}^t(\mathbf{H}\mathbf{R}_f\mathbf{H}^t + \mathbf{R}_z)^{-1})^t(\mathbf{R}_f\mathbf{H}^t(\mathbf{H}\mathbf{R}_f\mathbf{H}^t \\ &\quad + \mathbf{R}_z)^{-1}))^{-1}(\mathbf{R}_f\mathbf{H}^t(\mathbf{H}\mathbf{R}_f\mathbf{H}^t + \mathbf{R}_z)^{-1})^t \\ &= (\mathbf{H}\mathbf{R}_f\mathbf{H}^t + \mathbf{R}_z)(\mathbf{H}\mathbf{R}_f^2\mathbf{H}^t)^{-1}\mathbf{H}\mathbf{R}_f. \end{aligned} \quad (25)$$

Right multiplying both sides by  $\mathbf{R}_f\mathbf{H}^t$ , we get

$$\mathbf{H}\mathbf{R}_f\mathbf{H}^t = \mathbf{H}\mathbf{R}_f\mathbf{H}^t + \mathbf{R}_z. \quad (26)$$

Equation (26) suggests that since there is no constraint on  $\mathbf{H}$ , the joint computation of  $\mathbf{H}$  and  $\mathbf{W}$  leads to the entries of  $\mathbf{H}$  increasing without bound and hence masking out the effect of noise. This is due to the lack of an energy-conserving constraint on the observation filter and leads to an increase in SNR at the detector. Even though the entries of  $\mathbf{H}^*$  increase without bounds, the optimal  $\mathbf{H}^*$  possesses significant structure. To understand these structural properties of  $\mathbf{H}^*$ , in Subsection 3.C we compute the singular value decomposition (SVD) of  $\mathbf{H}$  and study the properties of singular values and the corresponding singular vectors. We then provide a procedure to design  $\mathbf{H}^*$  that satisfies Eq. (25) and consequently  $\mathbf{W}^*$ . The proposed optimal  $\mathbf{W}^*$  and  $\mathbf{H}^*$  satisfy Eqs. (23) and (24) and hence in turn satisfy Eq. (22). It turns out that there is not a unique solution. The proposed design procedure leads to a multitude of  $(\mathbf{H}^*, \mathbf{W}^*)$  solutions to the optimization problem as discussed in Subsection 3.C.

#### C. Proposed Optimal Filters

In this subsection, we present closed-form solutions for  $\mathbf{H}$  and  $\mathbf{W}$  in the unconstrained optimization problem. Let the SVD of the observation filter be  $\mathbf{H} = \mathbf{U}\Sigma_{\mathbf{H}}\mathbf{V}^t$ , where  $\mathbf{U}$  and  $\mathbf{V}$  are orthonormal matrices and  $\Sigma_{\mathbf{H}}$  is a  $m \times n$  matrix with the singular values of  $\mathbf{H}$  on the diagonal. Also, let the eigenvalue decomposition of  $\mathbf{R}_f$  and  $\mathbf{R}_z$  be given by  $\mathbf{R}_f = \mathbf{Q}_f\Lambda_f\mathbf{Q}_f^t$  and  $\mathbf{R}_z = \mathbf{Q}_z\Lambda_z\mathbf{Q}_z^t$ , respectively, where  $\mathbf{Q}_f$  and  $\mathbf{Q}_z$  are orthonormal matrices and  $\Lambda_f$  and  $\Lambda_z$  are diagonal matrices with the eigenvalues ordered as  $\lambda_{f_1} \leq \lambda_{f_2} \leq \dots \leq \lambda_{f_n}$  and  $\lambda_{z1} \leq \lambda_{z2} \leq \dots \leq \lambda_{zm}$ , respectively.

The design procedure for the optimal observation filter  $\mathbf{H}^*$  is as follows. The left singular vectors of  $\mathbf{H}^*$  are selected as

$$\mathbf{U} = \mathbf{Q}_z. \quad (27)$$

The singular values of  $\mathbf{H}^*$  are

$$\sigma_{H_i} \rightarrow \infty \quad \forall i = 1 \dots m. \quad (28)$$

The right singular vectors of  $\mathbf{H}^*$  are given by

$$\mathbf{V} = \mathbf{Q}_f \mathbf{P}_n, \quad (29)$$

where,  $\mathbf{P}_n$  is a permutation matrix of size  $n \times n$ . Further, we choose the permutation matrix  $\mathbf{P}_n$  to have the following structure:

$$\mathbf{P}_n = \begin{bmatrix} \mathbf{0} & \mathbf{P}_{n-m} \\ \mathbf{I}_m & \mathbf{0} \end{bmatrix}, \quad (30)$$

where  $\mathbf{I}_m$  is the identity matrix of size  $m$  and  $\mathbf{P}_{n-m}$  is an arbitrary permutation matrix of size  $(n-m) \times (n-m)$ . There are  $(n-m)!$  possible permutation matrices of size  $(n-m) \times (n-m)$ . Also, each of the elements of  $\mathbf{I}_m$  and  $\mathbf{P}_{n-m}$  can be positive or negative. Thus, we have  $2^n (n-m)!$  choices of permutation matrices that lead to multiple globally optimal observation filters  $\mathbf{H}^*$ . To prove that these design choices are a solution to the unconstrained optimization problem, we substitute our design choices into Eq. (25) as follows:

$$\begin{aligned} \mathbf{U} \Sigma_{\mathbf{H}} \mathbf{V}^t &= [(\mathbf{U} \Sigma_{\mathbf{H}} \mathbf{V}^t \mathbf{Q}_f \Lambda_f \mathbf{Q}_f^t \mathbf{V} \Sigma_{\mathbf{H}}^t \mathbf{U}^t + \mathbf{Q}_z \Lambda_z \mathbf{Q}_z^t) \\ &\quad (\mathbf{U} \Sigma_{\mathbf{H}} \mathbf{V}^t \mathbf{Q}_f \Lambda_f^2 \mathbf{Q}_f^t \mathbf{V} \Sigma_{\mathbf{H}}^t \mathbf{U}^t)^{-1} \\ &\quad \times (\mathbf{U} \Sigma_{\mathbf{H}} \mathbf{V}^t \mathbf{Q}_f \Lambda_f \mathbf{Q}_f^t)]. \end{aligned} \quad (31)$$

To find the singular values of  $\mathbf{H}$ , we simplify Eq. (31) using the design choices from Eqs. (27) and (29) and the orthogonality of  $\mathbf{Q}_f$  and  $\mathbf{Q}_z$ :

$$\begin{aligned} \Sigma_{\mathbf{H}} &= (\Sigma_{\mathbf{H}} \mathbf{P}_n^t \Lambda_f \mathbf{P}_n \Sigma_{\mathbf{H}}^t \\ &\quad + \Lambda_z) (\Sigma_{\mathbf{H}} \mathbf{P}_n^t \Lambda_f^2 \mathbf{P}_n \Sigma_{\mathbf{H}}^t)^{-1} \Sigma_{\mathbf{H}} \mathbf{P}_n^t \Lambda_f \mathbf{P}_n. \end{aligned} \quad (32)$$

Now, to explicitly evaluate  $\Sigma_{\mathbf{H}}$ , we need to understand the role of  $\mathbf{P}_n$  in Eq. (32). Recall that the eigenvalues of  $\Lambda_f$  are ordered as  $\lambda_{f_1} \leq \lambda_{f_2} \leq \dots \leq \lambda_{f_n}$ . Also, let the eigenvalues of  $\mathbf{R}_f$  be expressed as

$$\Lambda_f = \begin{bmatrix} \Lambda_{f_{n-m}} & \mathbf{0} \\ \mathbf{0} & \Lambda_{f_m} \end{bmatrix}, \quad (33)$$

where  $\Lambda_{f_{n-m}}$  is a diagonal matrix of size  $(n-m)$  with eigenvalues  $\lambda_{f_1} \dots \lambda_{f_{n-m}}$  on the diagonal and  $\Lambda_{f_m}$  is a square matrix of size  $m$  with eigenvalues  $\lambda_{f_{n-m+1}} \dots \lambda_{f_n}$  on the diagonal.

It is easy to see that right multiplying a diagonal matrix,  $\Lambda_f$ , by a permutation matrix  $\mathbf{P}_n$  and left multiplying the result by the transpose of  $\mathbf{P}_n$  leads to only a change in the order of the eigenvalues along the diagonal. Denote the product  $\mathbf{P}_n^t \Lambda_f \mathbf{P}_n$  by  $\Lambda_{f,\mathbf{P}}$ . From Eqs. (30) and (33), we can write  $\Lambda_{f,\mathbf{P}}$  as

$$\Lambda_{f,\mathbf{P}} = \mathbf{P}_n^t \Lambda_f \mathbf{P}_n = \begin{bmatrix} \Lambda_{f_m} & \mathbf{0} \\ \mathbf{0} & \mathbf{P}_{n-m}^t \Lambda_{f_{n-m}} \mathbf{P}_{n-m} \end{bmatrix}. \quad (34)$$

Similarly,

$$\Lambda_{f^2,\mathbf{P}} = \mathbf{P}_n^t \Lambda_f^2 \mathbf{P}_n = \begin{bmatrix} \Lambda_{f_m}^2 & \mathbf{0} \\ \mathbf{0} & \mathbf{P}_{n-m}^t \Lambda_{f_{n-m}}^2 \mathbf{P}_{n-m} \end{bmatrix}. \quad (35)$$

Rewriting the singular values of  $\mathbf{H}$  from Eq. (32) using Eqs. (34) and (35), we obtain

$$\Sigma_{\mathbf{H}} = (\Sigma_{\mathbf{H}} \Lambda_{f,\mathbf{P}} \Sigma_{\mathbf{H}}^t + \Lambda_z) (\Sigma_{\mathbf{H}} \Lambda_{f^2,\mathbf{P}} \Sigma_{\mathbf{H}}^t)^{-1} \Sigma_{\mathbf{H}} \Lambda_{f,\mathbf{P}}. \quad (36)$$

Expressing (36) elementwise,

$$\sigma_{H_i} = \frac{(\lambda_{f_{i+p}} \sigma_{H_i}^2 + \lambda_{z_i})(\lambda_{f_{i+p}} \sigma_{H_i})}{\lambda_{f_{i+p}}^2 \sigma_{H_i}^2} \quad \forall i = 1 \dots m. \quad (37)$$

Simplifying Eq. (37) implies that

$$\frac{\lambda_{z_i}}{\sigma_{H_i} \lambda_{f_{i+p}}} = 0 \quad \forall i = 1 \dots m, \quad (38)$$

where  $p = n - m$  is the shift in eigenvalues caused by the permutation matrix  $\mathbf{P}_n$ . Since both  $\lambda_{f_{i+p}}$  and  $\lambda_{z_i}$  are finite nonnegative numbers, we deduce that  $\sigma_{H_i}$  go to infinity, thereby making the entries of the matrix  $\mathbf{H}^*$  go to infinity. Thus, the proposed solution satisfies Eq. (25) and hence is optimal. The corresponding optimal reconstruction filter is the Wiener filter described in Eq. (23).

D. Lower Bound on MSE—Minimum MSE with Unconstrained  $\mathbf{H}$

According to the proposed design, we have  $2^n (n-m)!$  choices of permutation matrices, which lead to  $2^n (n-m)!$  possible optimal observation and reconstruction matrices  $\mathbf{H}^*$  and  $\mathbf{W}^*$ . Interestingly, even though we have multiple globally optimal solutions, the minima achieved by all these solutions are the same, i.e., they achieve the same minimum MSE.

**Proposition 2.** *The minimum MSE with the optimal choice for  $\mathbf{H}$  and  $\mathbf{W}$  for an unconstrained optimization is given by the sum of the least  $(n-m)$  eigenvalues of  $\mathbf{R}_f$ .*

*Proof.* Substituting  $\mathbf{W}$  as the Wiener filter from Eq. (8) into Eq. (7), we obtain the MSE in terms of  $\mathbf{H}$ ,  $\mathbf{R}_f$ , and  $\mathbf{R}_z$  as

$$J = \text{Tr}[\mathbf{R}_f - \mathbf{R}_f \mathbf{H}^t (\mathbf{R}_z + \mathbf{H} \mathbf{R}_f \mathbf{H}^t)^{-1} \mathbf{H} \mathbf{R}_f]. \quad (39)$$

From Eq. (26) we know that  $\mathbf{H}$  tends to infinity, and hence we can neglect the effect of noise. Hence, rewriting Eq. (39) without the noise term and simplifying, we obtain

$$= \text{Tr}[\mathbf{R}_f] - \text{Tr}[\mathbf{R}_f \mathbf{H}^t (\mathbf{H} \mathbf{R}_f \mathbf{H}^t)^{-1} (\mathbf{H} \mathbf{R}_f)]. \quad (40)$$

From Eq. (40), we can write the MSE expression as

$$J = \text{Tr}[\mathbf{R}_f] - \text{Tr}[\mathbf{X}], \quad (41)$$

where

$$\mathbf{X} = \mathbf{R}_f \mathbf{H}^t (\mathbf{H} \mathbf{R}_f \mathbf{H}^t)^{-1} (\mathbf{H} \mathbf{R}_f). \quad (42)$$

Making use of the proposed design procedure,  $\mathbf{V} = \mathbf{Q}_f \mathbf{P}$  and  $\mathbf{U} = \mathbf{Q}_z$ , we simplify Eq. (42) as

$$\text{Tr}[\mathbf{X}] = \text{Tr}[\mathbf{Q}_f \mathbf{\Lambda}_f \mathbf{P} \Sigma_{\mathbf{H}}^t (\Sigma_{\mathbf{H}} \mathbf{P}^t \mathbf{\Lambda}_f \mathbf{P} \Sigma_{\mathbf{H}}^t)^{-1} \Sigma_{\mathbf{H}} \mathbf{P}^t \mathbf{\Lambda}_f \mathbf{Q}_f^t]. \quad (43)$$

Substituting from Eq. (34) in Eq. (43), we obtain

$$\text{Tr}[\mathbf{X}] = \text{Tr}[\mathbf{Q}_f \mathbf{\Lambda}_f \mathbf{P} \Sigma_{\mathbf{H}}^t (\Sigma_{\mathbf{H}} \mathbf{\Lambda}_{f,p} \Sigma_{\mathbf{H}}^t)^{-1} \Sigma_{\mathbf{H}} \mathbf{P}^t \mathbf{\Lambda}_f \mathbf{Q}_f^t]. \quad (44)$$

Writing the above equation elementwise,

$$\text{Tr}[\mathbf{X}] = \sum_{i=1}^m \lambda_{f_{i+p}}^2 \sigma_{H_i}^2 (\sigma_{H_i}^2 \lambda_{f_{i+p}})^{-1} = \sum_{i=1}^m \lambda_{f_{i+p}}, \quad (45)$$

where  $p = n - m$ . Hence, from Eqs. (41) and (45),

$$J = \text{Tr} \begin{bmatrix} \lambda_{f_1} & 0 & \vdots & \vdots & 0 \\ 0 & \lambda_{f_2} & \vdots & \vdots & \vdots \\ \dots & \dots & \ddots & \vdots & \vdots \\ \dots & \dots & \dots & \ddots & \vdots \\ 0 & \dots & \dots & \dots & \lambda_{f_n} \end{bmatrix} - \text{Tr} \begin{bmatrix} 0 & 0 & 0 & 0 & 0 \\ 0 & 0 & 0 & 0 & 0 \\ 0 & 0 & \lambda_{f_{n-m+1}} & 0 & 0 \\ 0 & 0 & 0 & \ddots & 0 \\ 0 & \dots & \dots & \dots & \lambda_{f_n} \end{bmatrix}, \quad (46)$$

$$= \sum_{i=1}^n \lambda_{f_i} - \sum_{i=1}^m \lambda_{f_{i+p}} = \sum_{i=1}^{n-m} \lambda_{f_i}. \quad (47)$$

Hence, the minimum error according to the design choice is given by the sum of the least  $n - m$  eigenvalues of  $\mathbf{R}_f$ .  $\square$

In the special case when the observation filter  $\mathbf{H}$  is invertible and square, i.e.,  $m = n$ , the MSE equals zero. Note that the minimum MSE is limited by the dimensionality of the observation filter  $\mathbf{H}$ .

#### 4. Energy-Conserving Minimization

The unconstrained minimization computes the limits on the performance of any computational imaging system. To make the system physically realizable, we impose the energy-conserving constraint on the observation filter  $\mathbf{H}$  as described in Subsection 2.C.2. The energy-conserving optimization problem

is again solved by partitioning it into inner and outer minimization problems.

##### A. Inner Minimization for Energy-Conserving $\mathbf{H}_{ec}$

**Proposition 3.** For a given signal and noise autocorrelation  $\mathbf{R}_f$  and  $\mathbf{R}_z$ , and a fixed reconstruction filter  $\mathbf{W}$ , the optimal observation filter  $\mathbf{H}_{ec}^*$  that satisfies the constraint in Eq. (10) and minimizes the end-to-end MSE is given by

$$\mathbf{H}_{ec}^* = (\mathbf{W}^t \mathbf{W})^{-1} \mathbf{W}^t \left( \mathbf{R}_f - \frac{1}{\alpha} \mathbf{j}_{n \times n} + \frac{1}{\alpha} \mathbf{W} \mathbf{j}_{m \times n} \right) \mathbf{R}_f^{-1},$$

where  $\alpha = \mathbf{j}_{1 \times n} \mathbf{R}_f^{-1} \mathbf{j}_{n \times 1}$  is a scalar constant.

*Proof.* The inner optimization problem stated in Eq. (11) can be solved by the method of Lagrange multipliers. Define the new objective function as

$$J_{ec} = \text{Tr}[\mathbf{R}_f - 2\mathbf{W} \mathbf{H}_{ec} \mathbf{R}_f + \mathbf{W} \mathbf{H}_{ec} \mathbf{R}_f \mathbf{H}_{ec}^t \mathbf{W}^t + \mathbf{W} \mathbf{R}_z \mathbf{W}^t] + \lambda [\mathbf{H}_{ec} \mathbf{j}_{n \times 1} - \mathbf{j}_{m \times 1}], \quad (48)$$

where  $\lambda$  is the Lagrangian operator of dimension  $1 \times m$ . The partial derivative of  $J_{ec}$  with respect to  $\mathbf{H}_{ec}$  is given by

$$\frac{\partial J_{ec}}{\partial \mathbf{H}_{ec}} = -2\mathbf{W}^t \mathbf{R}_f + 2\mathbf{W}^t \mathbf{W} \mathbf{H}_{ec} \mathbf{R}_f + \lambda^t \mathbf{j}_{1 \times n} = 0, \quad (49)$$

$$\Rightarrow \mathbf{H}_{ec} = \frac{1}{2} (\mathbf{W}^t \mathbf{W})^{-1} (2\mathbf{W}^t \mathbf{R}_f - \lambda^t \mathbf{j}_{1 \times n}) \mathbf{R}_f^{-1}. \quad (50)$$

Substituting for  $\mathbf{H}_{ec}$  from Eq. (50) in the constraint (10), we find the Lagrangian operator as follows:

$$\begin{aligned} & \frac{1}{2} (\mathbf{W}^t \mathbf{W})^{-1} (2\mathbf{W}^t \mathbf{R}_f - \lambda^t \mathbf{j}_{1 \times n}) \mathbf{R}_f^{-1} \mathbf{j}_{n \times 1} \\ & = \mathbf{j}_{m \times 1} \Rightarrow \lambda^t = \frac{2}{\alpha} (\mathbf{W}^t \mathbf{j}_{n \times 1} - \mathbf{W}^t \mathbf{W} \mathbf{j}_{m \times 1}), \end{aligned} \quad (51)$$

where  $\alpha = \mathbf{j}_{1 \times n} \mathbf{R}_f^{-1} \mathbf{j}_{n \times 1}$  is a scalar constant that depends on signal autocorrelation. Substituting for  $\lambda$  in Eq. (50), we obtain

$$\mathbf{H}_{ec}^* = (\mathbf{W}^t \mathbf{W})^{-1} \mathbf{W}^t \left( \mathbf{R}_f - \frac{1}{\alpha} \mathbf{j}_{n \times n} + \frac{1}{\alpha} \mathbf{W} \mathbf{j}_{m \times n} \right) \mathbf{R}_f^{-1}. \quad (52)$$

We now solve the outer minimization problem with the energy conservation constraint.

##### B. Outer Minimization for Energy Conservation $\mathbf{H}_{ec}$ and $\mathbf{W}_{ec}$

Similarly to in the unconstrained case, we substitute the solution of the inner energy constrained minimization problem from Eq. (52) into Eq. (15)



to obtain the outer minimization problem, which is given by

$$\min_{\mathbf{W}_{ec}} \text{Tr} \left[ \mathbf{R}_f - \mathbf{W}_{ec} (\mathbf{W}_{ec}^t \mathbf{W}_{ec})^{-1} \mathbf{W}_{ec}^t \mathbf{R}_f + \frac{1}{\alpha^2} \mathbf{W}_{ec} (\mathbf{W}_{ec}^t \mathbf{W}_{ec})^{-1} \mathbf{W}_{ec}^t \mathbf{j}_{n \times n} \mathbf{R}_f^{-1} \mathbf{j}_{n \times n} - \frac{2}{\alpha^2} \mathbf{W}_{ec} \mathbf{j}_{m \times n} \mathbf{R}_f^{-1} \mathbf{j}_{n \times n} + \frac{1}{\alpha^2} \mathbf{W}_{ec} \mathbf{j}_{m \times n} \mathbf{R}_f^{-1} \mathbf{j}_{n \times m} \mathbf{W}_{ec}^t + \mathbf{W}_{ec} \mathbf{R}_z \mathbf{W}_{ec}^t \right] \quad (53)$$

The details of the substitution and the simplifications necessary to obtain Eq. (53) are given in Appendix . We now have an outer minimization problem over  $\mathbf{W}_{ec}$ , which we solve by setting the derivative of (53) with respect to  $\mathbf{W}_{ec}$  to zero. The detailed steps involved in the differentiation procedure are given in Appendix . Now, the goal is to obtain  $\mathbf{W}_{ec}$  from Eq. (A9) in terms of the input and noise autocorrelation  $\mathbf{R}_f$  and  $\mathbf{R}_z$ . Solving Eq. (A9) directly to obtain  $\mathbf{W}_{ec}$  is difficult. We make use of the following two equations to provide the solution:

$$\mathbf{W}_{ec}^* = \mathbf{R}_f \mathbf{H}_{ec}^t (\mathbf{H}_{ec} \mathbf{R}_f \mathbf{H}_{ec}^t + \mathbf{R}_z)^{-1}, \quad (54)$$

$$\mathbf{H}_{ec}^* = (\mathbf{W}_{ec}^t \mathbf{W}_{ec})^{-1} \mathbf{W}_{ec}^t \left( \mathbf{R}_f - \frac{1}{\alpha} \mathbf{j}_{n \times n} + \frac{1}{\alpha} \mathbf{W}_{ec} \mathbf{j}_{m \times n} \right) \mathbf{R}_f^{-1}. \quad (55)$$

In Appendix , we show that solving Eqs. (54) and (55) jointly is equivalent to solving Eq. (A9); i.e., if we substitute Eq. (55) into Eq. (54), we would obtain the exact same equation in  $\mathbf{W}_{ec}$ ,  $\mathbf{R}_f$ , and  $\mathbf{R}_z$  as Eq. (A9).

So, now we have to solve for the optimal  $(\mathbf{H}_{ec}^*, \mathbf{W}_{ec}^*)$  from Eqs. (54) and (55) jointly. We approach the problem in two ways, namely, the large SNR approximation and alternating minimization.

### C. Large SNR Approximation

We make a large SNR approximation, indicating that the signal power is much larger than the noise power, and provide closed-form solutions to energy-conserving optimization problem.

#### 1. Energy Conservation Solution

In this section, we present the solution to the energy conservation constrained optimization problem. The structure of the solution is similar to the unconstrained case. The left and the right singular vectors remain identical to the unconstrained solution, namely,

$$\mathbf{U}_{ec} = \mathbf{Q}_z, \quad \mathbf{V}_{ec} = \mathbf{Q}_f \mathbf{P}_n, \quad (56)$$

where  $\mathbf{P}_n$  is one of the  $2^n(n-m)!$  choices of permutation matrices as specified in Eq. (30).

To find the singular values of  $\mathbf{H}_{ec}$ , we substitute the SVD of  $\mathbf{H}$  into Eq. (10),

$$\mathbf{H}_{ec} \mathbf{j}_{n \times 1} = \mathbf{j}_{m \times 1} \Rightarrow \mathbf{U}_{ec} \Sigma_{\mathbf{H}_{ec}} \mathbf{V}_{ec}^t \mathbf{j}_{n \times 1} = \mathbf{j}_{m \times 1}. \quad (57)$$

Substituting the design choice from Eq. (56), we obtain

$$\begin{aligned} \mathbf{Q}_z \Sigma_{\mathbf{H}_{ec}} (\mathbf{Q}_f \mathbf{P}_n)^t \mathbf{j}_{n \times 1} &= \mathbf{j}_{m \times 1} \Rightarrow \Sigma_{\mathbf{H}_{ec}} \mathbf{P}_n^t \mathbf{Q}_f^t \mathbf{j}_{n \times 1} \\ &= \mathbf{Q}_z^t \mathbf{j}_{m \times 1}. \end{aligned} \quad (58)$$

Let  $\mathbf{P}_n^t \mathbf{Q}_f^t \mathbf{j}_{n \times 1} = \mathbf{a}$  and  $\mathbf{Q}_z^t \mathbf{j}_{m \times 1} = \mathbf{b}$ , where the dimensions of  $\mathbf{a}$  and  $\mathbf{b}$  are  $n \times 1$  and  $m \times 1$ , respectively. Now, we can solve for  $\sigma_i$  as

$$\sigma_{H_{eci}} = b_i / a_i \quad \forall i = 1 \dots m. \quad (59)$$

Hence, using the procedure described above we can completely design the observation matrix,  $\mathbf{H}_{ec} = \mathbf{U}_{ec} \Sigma_{\mathbf{H}_{ec}} \mathbf{V}_{ec}^t$ , given the knowledge of input and noise statistics. The optimal reconstruction filter can then be designed by using Eq. (54). In Appendix , we prove the optimality of this design procedure by showing that it satisfies Eqs. (54) and (55) jointly in the presence of the large SNR approximation. Note that, because of the permutation matrix  $\mathbf{P}_n$ , we again have multiple optimal solutions that lead to the same minima, i.e., the same minimum MSE. In the next subsection, we compute an analytical lower bound on the MSE with this choice of  $\mathbf{H}_{ec}^*$  and  $\mathbf{W}_{ec}^*$ .

#### 2. Minimum MSE with Energy-Conserving $\mathbf{H}_{ec}$

Now, we derive the MSE for the energy conservation constrained case by using the proposed optimal observation and reconstruction filters  $\mathbf{H}_{ec}^*$  and  $\mathbf{W}_{ec}^*$ .

**Proposition 4.** The minimum MSE with the optimal energy-conserving  $\mathbf{H}_{ec}$  and  $\mathbf{W}_{ec}$  is given by

$$\sum_{i=1}^n \lambda_{f_i} - \sum_{i=1}^m \lambda_{f_{i+p}} \left( \frac{\sigma_{H_{eci}}^2 \lambda_{f_{i+p}}}{\sigma_{H_{eci}}^2 \lambda_{f_{i+p}} + \lambda_{zi}} \right).$$

*Proof.* Rewrite the MSE from Eq. (48) as

$$J_{ec} = \text{Tr}[\mathbf{R}_f] - \text{Tr}[\mathbf{X}], \quad (60)$$

where

$$\mathbf{X} = \mathbf{R}_f \mathbf{H}_{ec}^t (\mathbf{H}_{ec} \mathbf{R}_f \mathbf{H}_{ec}^t + \mathbf{R}_z)^{-1} (\mathbf{H}_{ec} \mathbf{R}_f). \quad (61)$$

Substituting the design choices into Eq. (61), the trace of  $\mathbf{X}$  is given as

$$\begin{aligned} \text{Tr}[\mathbf{X}] &= \text{Tr}[\mathbf{Q}_f \mathbf{\Lambda}_f \mathbf{P}_n \Sigma_{\mathbf{H}_{ec}}^t (\Sigma_{\mathbf{H}_{ec}} \mathbf{P}_n^t \mathbf{\Lambda}_f \mathbf{P}_n \Sigma_{\mathbf{H}_{ec}}^t \\ &\quad + \mathbf{\Lambda}_z)^{-1} \Sigma_{\mathbf{H}_{ec}} \mathbf{P}_n^t \mathbf{\Lambda}_f \mathbf{Q}_f^t]. \end{aligned}$$

Further simplifying from Eq. (34), we obtain

$$\begin{aligned} \text{Tr}[\mathbf{X}] &= \text{Tr}[\mathbf{Q}_f \mathbf{\Lambda}_f \mathbf{P}_n \Sigma_{\mathbf{H}_{ec}}^t (\Sigma_{\mathbf{H}_{ec}} \mathbf{\Lambda}_f \mathbf{P}_n \Sigma_{\mathbf{H}_{ec}}^t \\ &\quad + \mathbf{\Lambda}_z)^{-1} \Sigma_{\mathbf{H}_{ec}} \mathbf{P}_n^t \mathbf{\Lambda}_f \mathbf{Q}_f^t]. \end{aligned}$$

Writing the above equation elementwise,

$$\text{Tr}[\mathbf{X}] = \sum_{i=1}^m \lambda_{f_{i+p}}^2 \sigma_{H_{eci}}^2 (\sigma_{H_{eci}}^2 \lambda_{f_{i+p}} + \lambda_{zi})^{-1},$$

where  $p = n - m$  is the shift caused by the permutation matrix  $\mathbf{P}_n$ . Hence, the minimum MSE is given by

$$\begin{aligned} J_{ec} &= \text{Tr}[\mathbf{R}_f] - \text{Tr}[\mathbf{X}] \\ &= \sum_{i=1}^n \lambda_{f_i} - \sum_{i=1}^m \lambda_{f_{i+p}}^2 \sigma_{H_{eci}}^2 (\sigma_{H_{eci}}^2 \lambda_{f_{i+p}} + \lambda_{zi})^{-1} \\ &= \sum_{i=1}^n \lambda_{f_i} - \sum_{i=1}^m \lambda_{f_{i+p}} \left( \frac{\sigma_{H_{eci}}^2 \lambda_{f_{i+p}}}{\sigma_{H_{eci}}^2 \lambda_{f_{i+p}} + \lambda_{zi}} \right), \end{aligned} \quad (62)$$

where  $\sigma_{H_{eci}} = b_i/a_i \times$  and is dependent of  $\mathbf{R}_f$  and  $\mathbf{R}_z$ .  $\square$

Taking the difference between the minimum MSE obtained from unconstrained  $\mathbf{H}$  in Eq. (47) and the minimum MSE obtained from energy-conserving  $\mathbf{H}_{ec}$  in Eq. (62),

$$\begin{aligned} J_{ec} - J &= \left[ \sum_{i=1}^n \lambda_{f_i} - \sum_{i=1}^m \lambda_{f_{i+p}} \left( \frac{\sigma_{H_{eci}}^2 \lambda_{f_{i+p}}}{\sigma_{H_{eci}}^2 \lambda_{f_{i+p}} + \lambda_{zi}} \right) \right] \\ &\quad - \left[ \sum_{i=1}^n \lambda_{f_i} - \sum_{i=1}^m \lambda_{f_{i+p}} \right] \end{aligned} \quad (63)$$

$$= \sum_{i=1}^m \lambda_{f_{i+p}} - \sum_{i=1}^m \lambda_{f_{i+p}} \left( \frac{\sigma_{H_{eci}}^2 \lambda_{f_{i+p}}}{\sigma_{H_{eci}}^2 \lambda_{f_{i+p}} + \lambda_{zi}} \right). \quad (64)$$

Since the term in parenthesis in Eq. (64) is less than 1, the minimum MSE with energy-conserving  $\mathbf{H}$  is clearly greater than the minimum MSE with unconstrained  $\mathbf{H}$ . Also, we observe that the MSE for both cases can be computed in closed form from  $\mathbf{R}_f$  and  $\mathbf{R}_z$ . With the large SNR approximation, the term in parenthesis in Eq. (64) equals 1. This implies that the energy-conserving minimum MSE with the large SNR approximation equals the minimum MSE obtained in the unconstrained case.

#### D. Alternating Minimization

We now propose an iterative process based on the well-known double minimization method [21] to compute optimal  $\mathbf{H}_{ec}$  and  $\mathbf{W}_{ec}$  jointly for arbitrary SNR. Let  $\mathbf{H}_{alt}$  and  $\mathbf{W}_{alt}$  denote the observation and reconstruction filters that are obtained from the alternating minimization procedure and satisfy the energy-conserving constraint. The iterative process consists of the following steps:

1. Start with any arbitrary  $\mathbf{H}_{alt1}$  matrix that belongs to the set  $\mathcal{H}_{ec}$  from Eq. (10). Set the iteration number  $i = 1$ .
2. Compute  $\mathbf{W}_{alti}$  for this observation matrix  $\mathbf{H}_{alti}$  by using Eq. (54).
3. Compute  $\mathbf{H}_{alti+1}$  for the reconstruction matrix  $\mathbf{W}_{alti}$  by using Eq. (55).
4. After the  $i$ th iteration, the MSE is given by

$$\begin{aligned} J_{alti} &= \text{Tr}[\mathbf{R}_f - 2\mathbf{W}_{alti} \mathbf{H}_{alti} \mathbf{R}_f + \mathbf{W}_{alti} \mathbf{H}_{alti} \mathbf{R}_f \mathbf{H}_{alti}^t \mathbf{W}_{alti}^t \\ &\quad + \mathbf{W}_{alti} \mathbf{R}_z \mathbf{W}_{alti}^t]. \end{aligned} \quad (65)$$

5. Set  $i = i + 1$ . Repeat steps 2 to 5 until a desired stopping condition is met.

A standard threshold stopping criteria based on successive difference in  $J_{alti}$  is used. The convergence of this iterative process is depicted in Fig. 2, which plots the variation of the MSE with number of iterations. Clearly, the algorithm converges within a few iterations to the optimal solution. We found that the iterative process converges for all initial values of  $\mathbf{H}_{alt}$  and for both colored and white noise cases.

In the next section, we describe the procedure to construct physically realizable observation filters commonly used in optical systems and contrast their performance with the proposed optimal filters.

#### 5. Physically Realizable, Traditional (Typical) Observation Filters

Typically, traditional optical system designs aim to maximize the energy at the detector or create a diffraction-limited image of the input at the detector. In contrast to this, the proposed filters minimize the end-to-end MSE between the input and the reconstructed image and optimize the performance of the overall system. We compare the performance of the proposed filters with off-the-shelf observation filters to study the limits on the performance of current state-of-the-art imaging systems and explore the possibility of improvement. Let observation matrix  $\mathbf{H}_{ots}$  represent a diffraction-limited imaging system that can be easily built and is commonly used in conventional imaging systems.

In this subsection, we also describe a method to compute an observation matrix  $\mathbf{H}_{nec}$  in which, in addition to its rows summing to unity, all its elements are nonnegative (one of the properties that makes the filter physically realizable) as indicated

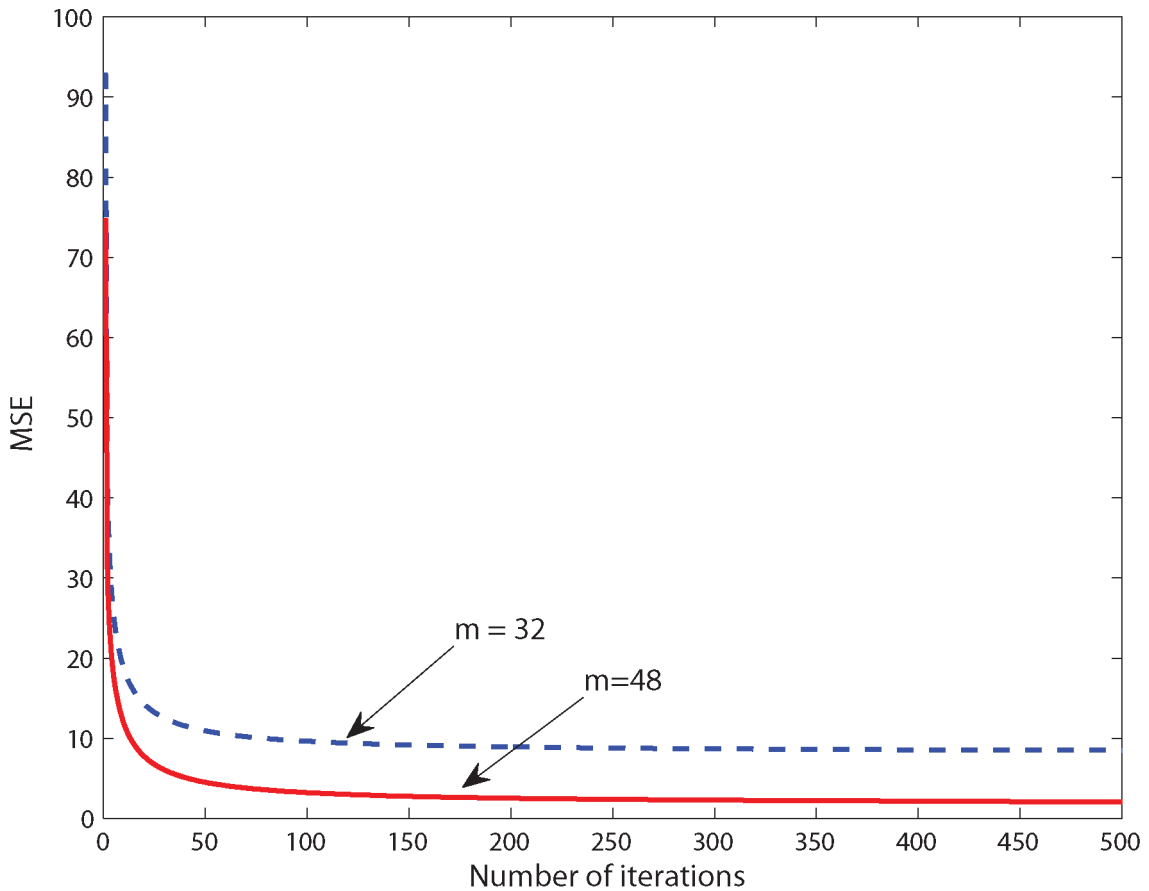


Fig. 2. (Color online) Convergence of MSE for alternating minimization procedure.

4/CO

in Section 2.C.2.  $\mathbf{H}_{\text{nec}}$  is computed by using a numerical optimization routine in MATLAB. It turns out that when  $\mathbf{H}_{\text{nec}}$  is used as the observation matrix in our simulations there is only a marginal reduction in peak SNR (PSNR) as compared with  $\mathbf{H}_{\text{ec}}$ , and it is a simple yet effective method to generate an observation matrix with all its elements being nonnegative and the rows summing to unity. In Section 6, we apply these physically realizable observation matrices to a few test images and compare the performance with the proposed jointly optimized filters.

#### A. “Off-the-Shelf” $\mathbf{H}_{\text{ots}}$

We denote by the off-the-shelf observation matrix  $\mathbf{H}_{\text{ots}}$  an observation matrix that represents the effect of a physically realizable optical system. We consider a lens with a rectangular aperture of size  $D$  meters. The focal length of the lens is denoted  $f_o$ , which implies that the  $f$ -number  $F/\# = f_o/D$  [22]. If the wavelength of light is denoted  $\lambda$ , the diffraction-limited spot size is given by  $\lambda F/\#$ . In a typical optical system, the  $F/\#$  usually ranges from 1 to 20. The smaller the  $F/\#$ , the tighter the spot size and higher the resolving power of the lens. The optical system corresponding to  $F/\# = 1$  can be considered a state-of-the-art optical system. Since the illumination is

incoherent, the point spread function is the squared modulus of the Fourier transform of the pupil function. The pupil function is simply a function that takes on a value of 1 inside the aperture, and 0 outside. Thus, the intensity point spread function of a rectangular aperture is the sinc squared function, which is low pass in the frequency domain. The effective observation matrix  $\mathbf{H}_{\text{ots}}$  is obtained by appropriately sampling the sinc squared function according to the number of observations at the detector  $m$ . Each row of  $\mathbf{H}_{\text{ots}}$  is a shifted version of each other (isoplanatic) and is appropriately scaled such that it sums to unity (energy conservation). Note that we assume that the system is diffraction limited and that the lens does not introduce any distortions, i.e., we assume an ideal optical system. The presence of distortions such as pin-cushion or barrel distortion causes further degradation in performance of the optical system [22]. In Section 6,  $\mathbf{H}_{\text{ots}}$  is applied to a few test images to gather images at the detector. The detected images are then reconstructed by using the Wiener filter from Eq. (8) corresponding to the observation filter  $\mathbf{H}_{\text{ots}}$ . PSNR values obtained by this method are then compared with the performance of the proposed optimal filters.

### B. Nonnegativity $\mathbf{H}_{\text{nec}}$

As discussed in Section 2, in addition to the requirement that the rows of the observation matrix sum to 1, we also need that all the elements of the observation matrix be nonnegative. In Section 2, we denoted such a matrix by  $\mathbf{H}_{\text{nec}}$  which would be obtained by solving optimization problem (13). The problem posed in Eq. (13) is convex in  $\mathbf{H}_{\text{nec}}$  defined over the intersection of sets  $\mathcal{H}_{\text{ec}}$  and  $\mathcal{H}_{\text{nneg}}$ , with  $\mathbf{W}_{\text{nec}}$  fixed. But, the problem is not convex over  $\mathbf{H}_{\text{nec}}$  and  $\mathbf{W}_{\text{nec}}$  jointly. This jointly nonconvex problem cannot be solved in a manner similar to the energy conservation optimization by utilizing generalized Benders' decomposition, since the inner minimization problem (optimizing over  $\mathbf{H}_{\text{nec}}$  with  $\mathbf{W}_{\text{nec}}$  fixed) involves a large number of inequality constraints and cannot be solved in closed form.

A numerical optimization software like MATLAB is used to solve the nonconvex optimization with inequality and equality constraints. It turns out that the increase in MSE as compared with the MSE obtained by  $\mathbf{H}_{\text{ec}}$  due to this numerical optimization is marginal.

## 6. Performance Analysis

In this section, the performance of the proposed jointly optimized observation and reconstruction filters is demonstrated. A few test images such as an aerial airport image and the Lena image are used for illustration. We use the PSNR, which can be computed from the MSE as

$$\text{PSNR} = 10 \log_{10} \left( 255^2 / \text{MSE} \right), \quad (66)$$

to objectively quantify the performance of the filters. The visual quality of the image after reconstruction is also used to judge the effectiveness of the filters. The size of the input image is  $(256 \times 256)$ , which we process in blocks of size  $(8 \times 8)$  to ease the computational complexity.

Recognize that the proposed energy-conserving optimal filters  $\mathbf{H}_{\text{ec}}$  can be designed in closed form and hence are easy to compute for large image sizes. However, the computational complexity associated with the performance analysis comes from the nonnegative  $\mathbf{H}_{\text{nec}}$ , which involves optimization via MATLAB. Since the number of variables increases to the second order with block sizes, it is difficult to compute these observation filters  $\mathbf{H}_{\text{nec}}$  for large image sizes. Hence, block sizes of  $(8 \times 8)$  are chosen to keep an even comparison.

These blocks when vectorized form vectors of length  $n = 64$ . The autocorrelation matrix  $\mathbf{R}_f$  of size  $n \times n$  is computed by averaging over all the vectorized blocks from the image. We add white noise of zero mean and variance given by  $\lambda_z^2$ . Thus, the noise autocorrelation matrix is  $\mathbf{R}_z = \lambda_z^2 \mathbf{I}_m$ , where  $\mathbf{I}_m$  is an identity matrix of size  $m \times m$ . The value of  $m$  is varied from  $m = 8$  to  $m = 64$ , depending on the number

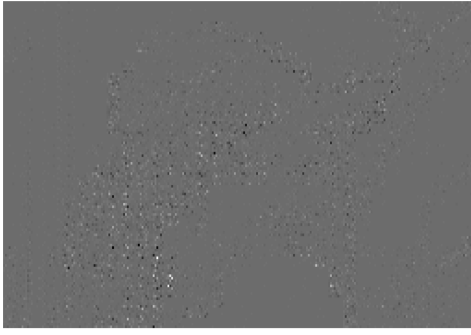
of pixels at the detector. Thus, the dimensions of the observation matrix are  $m \times 64$ .

### A. Image Reconstruction

To demonstrate the performance of the proposed jointly designed optimal filters, the observation matrix  $\mathbf{H}_{\text{ec}}$  obtained by the large SNR approximation from Subsection 4.C.1 is applied to the test images. The resulting image at the detector  $\mathbf{g}$  is observed. The reconstructed image  $\hat{\mathbf{f}}$  is then obtained by applying the optimal reconstruction filter  $\mathbf{W}_{\text{ec}}$  to  $\mathbf{g}$ . The noise variance for this experiment is fixed at  $\lambda_z^2 = 1$ . The number of pixels at the detector is chosen to be  $m = 32$ , which implies that for every 64 pixels in the original scene, we have only 32 blurred pixels at the detector. As with any typical computational imager, we expect the image of the scene to be indiscernible at the output of the detector. This is because the observation filter is designed for end-to-end optimality, which implies that the reconstructed image will be as close as possible to the source image, whereas the detected image need not be a good image of the source. The detected images  $\mathbf{g}$  for the Lena and aerial images are shown in Figs. 3(a) and 4(a), respectively. The detected output images are then reconstructed by using the Wiener filter from Eq. (8) and are shown in Figs. 3(b) and 4(b). We observe that the reconstructed images have a high visual quality and PSNR values of 38.2337 and 38.5194, respectively. In Figs. 3(c) and 4(c), we display the reconstructed image obtained by applying the  $\mathbf{H}_{\text{nec}}$  to the Lena and the aerial airport image. There is only a slight reduction (around 1.5 dB) in the PSNR of the reconstructed image by utilizing  $\mathbf{H}_{\text{nec}}$  instead of the energy-conserving  $\mathbf{H}_{\text{ec}}$ . Recognize that  $\mathbf{H}_{\text{nec}}$  satisfies the additional constraint of all its elements being nonnegative. Since the solution space is more constrained, the PSNR obtained is lower as compared with  $\mathbf{H}_{\text{ec}}$ .  $\mathbf{H}_{\text{nec}}$  is closer to physically realizable optical systems and can be used in the design of a computational imaging system with only a slight loss (reduction) in PSNR.

To compare the performance of the proposed filters with the current optical systems, we construct an off-the-shelf  $\mathbf{H}_{\text{ots}}$ . The  $F/\#$  of the lens is chosen to be 1, which represents a state-of-the-art optical system. The wavelength of light is assumed to be  $\lambda = 550$  nm (center of the visible spectrum), and hence the diffraction-limited spot size turns out to be  $0.55 \mu\text{m}$ . We construct an observation matrix  $\mathbf{H}_{\text{ots}}$  with this spot size as described in Section 5. Note that we have considered that the detector pixel size is equal to the spot size in our simulations. Current imaging devices have the smallest detector pixel size around  $2 \mu\text{m}$ . We have thus created an off-the-shelf observation matrix that is very aggressive and performs extremely well. The reconstructed image obtained by applying the real off-the-shelf  $\mathbf{H}_{\text{ots}}$  is shown in Figs. 3(d) and 4(d). The PSNR of the reconstructed aerial airport image is 34.5474, which is around 3.9 dB less than that obtained by the





(a)



(b)



(c)



(d)



(e)

Fig. 3. (a) Detected Lena image. (b) Reconstructed Lena image, PSNR = 38.2337. (c) Reconstructed Lena image,  $\mathbf{H}_{\text{nec}}$ , PSNR = 36.9964. (d) Reconstructed image,  $\mathbf{H}_{\text{ots}}$ , spot size =  $0.55 \mu\text{m}$ , PSNR = 36.4454. (e) Reconstructed image,  $\mathbf{H}_{\text{ots}}$ , spot size =  $1.3 \mu\text{m}$ , PSNR = 33.7098.

energy-conserving observation matrix  $\mathbf{H}_{\text{ec}}$ . For the Lena image the difference in PSNR is 1.7 dB. This difference in PSNR shows that even when  $\mathbf{H}_{\text{ots}}$  with  $F/\# = 1$  is used, there is still a possibility for improvement that can be exploited to create superior imaging systems. We also show reconstructed images of Lena and the aerial airport image when an observation matrix  $\mathbf{H}_{\text{ots}}$  with  $F/\# = 2.5$ , which corresponds to a spot size of  $1.3 \mu\text{m}$ , is used in Figs. 3(e) and 4(e). We observe that the visual quality as well as the PSNR of these images is significantly lower than that obtained by using  $\mathbf{H}_{\text{ec}}$ . In the following section, we

show the variation of PSNR with the number of pixels at the detector.

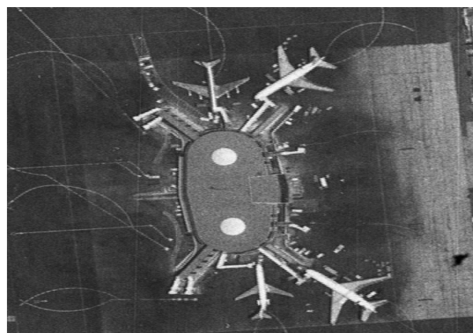
## B. Comparison of Performance of Optimal Observation Filter $\mathbf{H}_{\text{ec}}^*$ with Unoptimized Physically Realizable Observation Filters

### 1. Variation of PSNR with Number of Pixels at the Detector

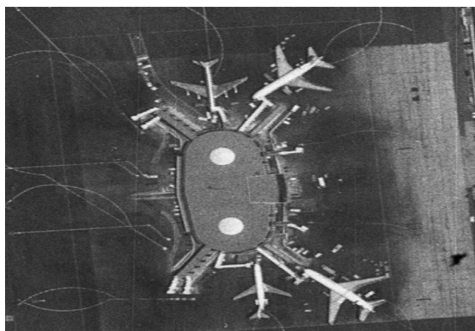
The PSNR of the proposed filters is evaluated for varying number of pixels at the detector  $m$  and



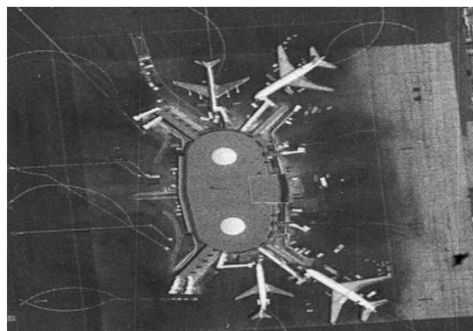
(a)



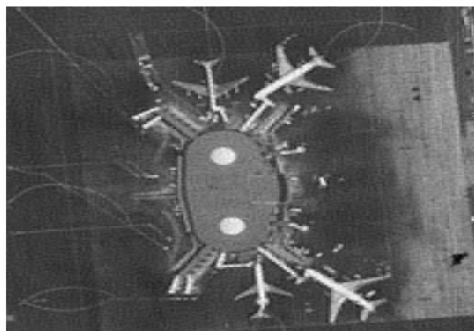
(b)



(c)



(d)



(e)

Fig. 4. (a) Detected airport image. (b) Reconstructed airport image,  $\text{PSNR} = 38.5194$ . (c) Reconstructed airport image,  $\mathbf{H}_{\text{nec}}$ ,  $\text{PSNR} = 36.7812$ . (d) Reconstructed airport image,  $\mathbf{H}_{\text{ots}}$ , spot size =  $0.55 \mu\text{m}$ ,  $\text{PSNR} = 34.5474$ . (e) Reconstructed airport image,  $\mathbf{H}_{\text{ots}}$ , spot size =  $1.3 \mu\text{m}$ ,  $\text{PSNR} = 33.8328$ .

two different noise variance values of  $\lambda_z^2 = 1$  and  $\lambda_z^2 = 10$ . In Section 5, we described methods to create a physically realizable observation matrix off-the-shelf  $\mathbf{H}_{\text{ots}}$  as well as an observation matrix that has all its elements nonnegative  $\mathbf{H}_{\text{nec}}$ . We now compare the performance of systems obtained by utilizing such observation matrices to the performance of the proposed jointly optimized system. As before, we generate two observation matrices  $\mathbf{H}_{\text{ots}}$  with different spot sizes, namely,  $0.55 \mu\text{m}$  and  $1.3 \mu\text{m}$ , which correspond to lenses with  $F/\#$  1 and 2.5, respectively. As described in Section 5, the smaller the spot size,

the better the optical system. In Fig. 5, we plot the variation of PSNR with  $m$  with the noise variance fixed at  $\lambda_z^2 = 1$ . The value of  $m$  varies from  $m = 8$  to  $m = 64$ . As  $m$  increases, the number of pixels at the detector becomes higher, which in turn means that more light (a greater number of photons) is gathered by the lens, leading to an increase in PSNR. The observation filter  $\mathbf{H}_{\text{alt}}$  obtained by the alternating minimization procedure described in Subsection 4.D performs almost identically to the unconstrained  $\mathbf{H}$ . We know that the solution to the unconstrained optimization is a universal bound

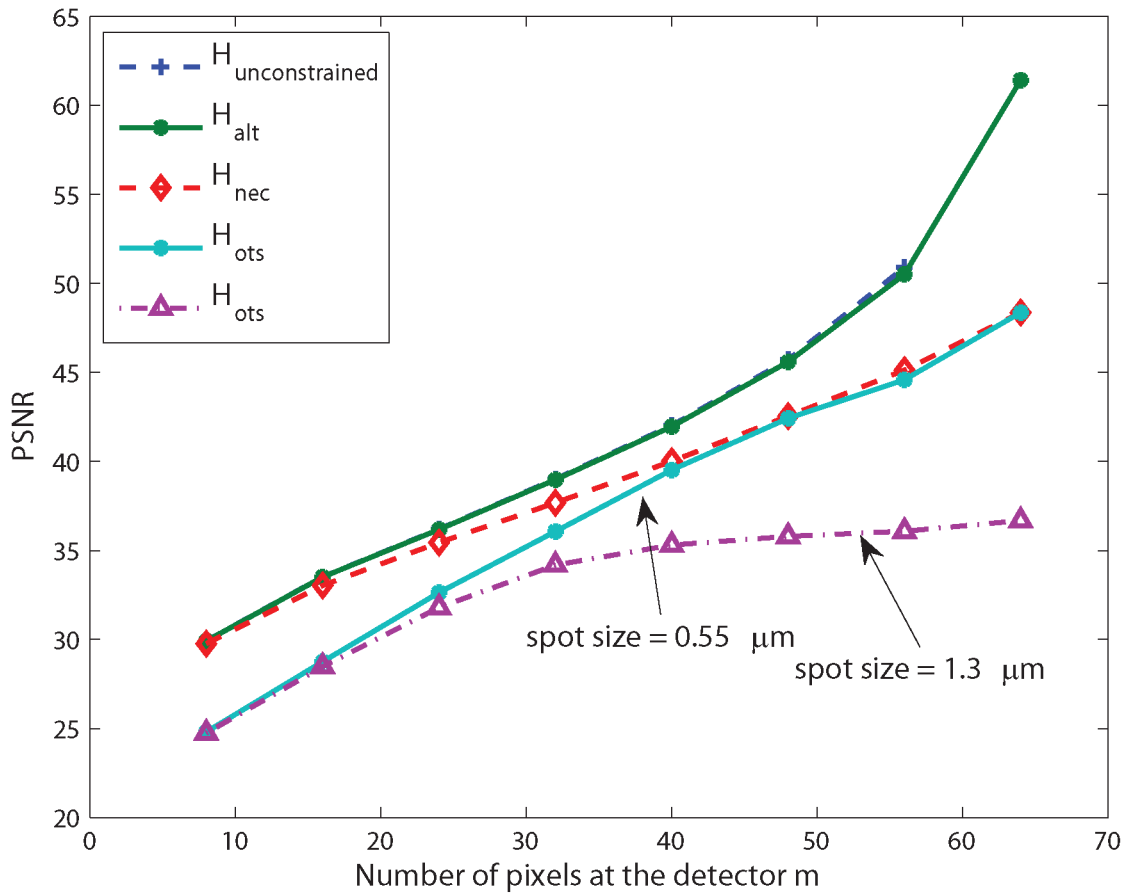


Fig. 5. (Color online) PSNR versus number of pixels at the detector  $m$ ,  $\lambda_z^2 = 1$ .

4/CO

on the performance of any computational imaging system. The performance of observation filters  $H_{\text{nec}}$  and  $H_{\text{ots}}$ , which satisfy energy conservation as well as all elements being positive constraint is also plotted. As the number of pixels at the detector  $m$  increases, the performance of  $H_{\text{nec}}$  and  $H_{\text{ots}}$  with spot size  $0.55 \mu\text{m}$  is close. At  $m = n = 64$ , the observation matrix becomes square and the performance of  $H_{\text{nec}}$  and  $H_{\text{ots}}$  with  $F/\# = 1$  is identical. But at low values of  $m$ , which is the case of interest, it can be clearly seen from Fig. 5 that  $H_{\text{nec}}$  gives a higher PSNR than the state-of-the-art optical systems. This gap in PSNR indicates the scope of improvement for current state-of-the-art optical systems. Note that  $H_{\text{nec}}$  uses the knowledge of signal and noise autocorrelations whereas  $H_{\text{ots}}$  is designed completely independently of any prior knowledge. The current state-of-the-art imaging systems can be improved by using an adaptive framework (PANOPTES) that steers the field of view of the optics based on scene content [9].

In Fig. 6, we plot the performance of  $H_{\text{ec}}$ ,  $H_{\text{nec}}$ , and  $H_{\text{ots}}$  for noise variance  $\lambda_z^2 = 10$ . Although the maximum PSNR attained is less than that obtained with  $\lambda_z^2 = 1$ , due to the presence of more noise in the system, we observe that the curves have performance similar to that of  $\lambda_z^2 = 1$ . As before, the performance

of alternating minimization filters corresponding to  $H_{\text{alt}}$  is close to the unconstrained system.

The system corresponding to  $F/\# = 2.5$ , which has a spot size closer to the current detector pixel size, has significantly lower performance than the systems corresponding to  $H_{\text{nec}}$  and  $H_{\text{ots}}$  with  $F/\# = 1$ . Note that, at  $m = 64$ , the unconstrained MSE is zero, which implies that the PSNR is infinity and hence is not plotted in Figs. 5 and 6.

## 2. Variation of PSNR with Noise Variance

The performance of  $H_{\text{ec}}$  with the large SNR approximation as described in Subsection 4.C.1 is demonstrated. In Fig. 7, the performance of unconstrained observation filter  $H$ , alternating minimization  $H_{\text{alt}}$ , energy-conserving  $H_{\text{ec}}$ , and nonnegative  $H_{\text{nec}}$  is plotted against the inverse of noise variance for  $m = 16$ . As expected, the performance of the unconstrained and the alternating minimization is nearly identical and defines the limits on the performance of this system. As the noise variance reduces, the large SNR approximation becomes valid and the optimal  $H_{\text{ec}}$  has PSNR values very close to unconstrained  $H$  and  $H_{\text{alt}}$ . The observation filter  $H_{\text{nec}}$  also approaches the maximum possible PSNR as the noise variance reduces. In

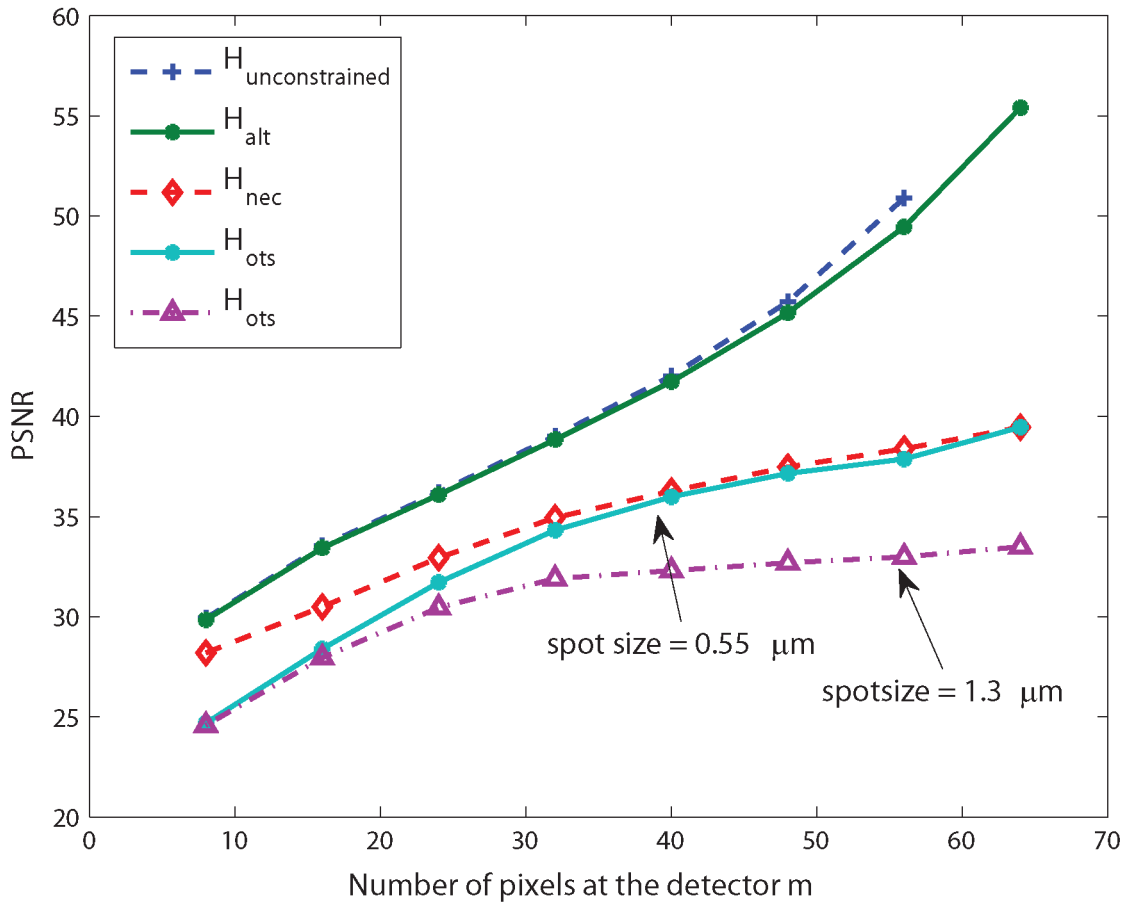


Fig. 6. (Color online) PSNR versus number of pixels at the detector  $m$ ,  $\lambda_z^2 = 10$ .

4/CO

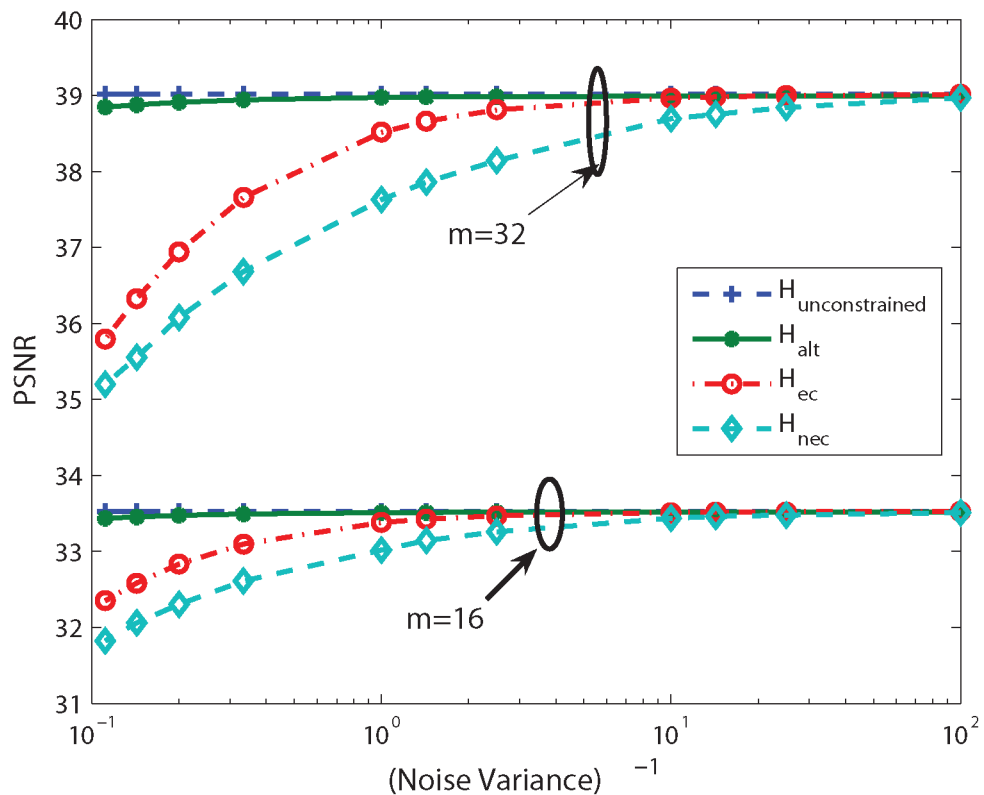


Fig. 7. (Color online) PSNR versus inverse of noise variance,  $m = 16$  and  $m = 32$ .

4/CO



Fig. 7, we also plot PSNR against the inverse of noise variance for  $m = 32$ . The overall performance of all the observation filters is higher than the  $m = 16$  case, as there are more pixels at the detector for a given number of input pixels. As the noise variance reduces,  $\mathbf{H}_{ec}$  asymptotically achieves the maximum PSNR, because the observation filter  $\mathbf{H}_{ec}$  is optimal with large SNR approximation.  $\mathbf{H}_{nec}$  also asymptotically achieves the maximum PSNR, though slower than  $\mathbf{H}_{ec}$ , because it satisfies the additional constraint of all elements being nonnegative.

## 7. Conclusions

This paper presented a framework for optimal code-design of a computational imaging system. We proposed a design procedure for the design of the observation and reconstruction filter that minimizes the end-to-end metric in closed form. The proposed filters are globally optimal and achieve the minimum MSE even though the optimization problem is not convex. The unconstrained optimization procedure in the proposed framework defines a lower bound on the performance of any computational imaging system. Further, to make the observation filter physically realizable, we imposed the physical constraint of energy conservation of the optical system. We also showed that there exist a multitude of globally optimal solutions to both the unconstrained and energy constrained optimization problems. The proposed design is applicable to white as well as colored noise.

Future work in this area includes imposing additional constraints on the observation filter to bring it to the stage where the system can actually be built. The observation filter  $\mathbf{H}$  can be represented as  $\mathbf{H} = \mathbf{H}_{det}\mathbf{H}_{lens}$ , where  $\mathbf{H}_{det}$  represents the effect of the detector and  $\mathbf{H}_{lens}$  represents the effect of

the lens. This decomposition gives a better handle for optimization, as constraints that are specific to the optics can be imposed on  $\mathbf{H}_{lens}$ . Another area that needs to be explored is the presence of signal-dependent noise in images captured by CCD and CMOS sensors [23].

## Appendix A: Energy Constrained Outer Minimization

In this appendix, we describe the procedure of substitution of the solution of the energy constrained inner minimization problem to obtain the outer problem. We then show the differentiation of the outer problem with respect to  $\mathbf{W}_{ec}$  to obtain the globally optimal  $(\mathbf{H}_{ec}^*, \mathbf{W}_{ec}^*)$ . Now, substituting Eq. (52) into Eq. (15), we obtain

$$J = \text{Tr} \left[ \mathbf{R}_f - 2\mathbf{W}(\mathbf{W}^t\mathbf{W})^{-1}\mathbf{W}^t \left( \mathbf{R}_f - \frac{1}{\alpha}\mathbf{j}_{n \times n} + \frac{1}{\alpha}\mathbf{W}\mathbf{j}_{m \times n} \right) + \mathbf{A} + \mathbf{W}\mathbf{R}_z\mathbf{W}^t \right], \quad (\text{A1})$$

where

$$\mathbf{A} = \mathbf{W}(\mathbf{W}^t\mathbf{W})^{-1}\mathbf{W}^t \left( \mathbf{R}_f - \frac{1}{\alpha}\mathbf{j}_{n \times n} + \frac{1}{\alpha}\mathbf{W}\mathbf{j}_{m \times n} \right) \mathbf{R}_f^{-1}\mathbf{R}_f\mathbf{R}_f^{-1} \times \left( \mathbf{R}_f - \frac{1}{\alpha}\mathbf{j}_{n \times n} + \frac{1}{\alpha}\mathbf{j}_{n \times m}\mathbf{W}^t \right) \mathbf{W}(\mathbf{W}^t\mathbf{W})^{-1}\mathbf{W}^t. \quad (\text{A2})$$

Using the cyclic property of trace, i.e.,  $\text{Tr}(\mathbf{XYZ}) = \text{Tr}(\mathbf{YZX})$ , we obtain

$$\begin{aligned} \text{Tr}[\mathbf{A}] &= \text{Tr} \left[ \mathbf{W}^t \left( \mathbf{R}_f - \frac{1}{\alpha}\mathbf{j}_{n \times n} + \frac{1}{\alpha}\mathbf{W}\mathbf{j}_{m \times n} \right) \mathbf{R}_f^{-1} \left( \mathbf{R}_f - \frac{1}{\alpha}\mathbf{j}_{n \times n} + \frac{1}{\alpha}\mathbf{j}_{n \times m}\mathbf{W}^t \right) \mathbf{W}(\mathbf{W}^t\mathbf{W})^{-1} \right] \\ &= \text{Tr} \left[ \left( \mathbf{R}_f - \frac{1}{\alpha}\mathbf{j}_{n \times n} + \frac{1}{\alpha}\mathbf{W}\mathbf{j}_{m \times n} \right) \mathbf{R}_f^{-1} \left( \mathbf{R}_f - \frac{1}{\alpha}\mathbf{j}_{n \times n} + \frac{1}{\alpha}\mathbf{j}_{n \times m}\mathbf{W}^t \right) \mathbf{W}(\mathbf{W}^t\mathbf{W})^{-1}\mathbf{W}^t \right] \\ &= \text{Tr} \left[ \left( \mathbf{I} - \frac{1}{\alpha}\mathbf{j}_{n \times n}\mathbf{R}_f^{-1} + \frac{1}{\alpha}\mathbf{W}\mathbf{j}_{m \times n}\mathbf{R}_f^{-1} \right) \left( \mathbf{R}_f - \frac{1}{\alpha}\mathbf{j}_{n \times n} + \frac{1}{\alpha}\mathbf{j}_{n \times m}\mathbf{W}^t \right) \mathbf{W}(\mathbf{W}^t\mathbf{W})^{-1}\mathbf{W}^t \right] \\ &= \text{Tr} \left[ \left( \mathbf{R}_f - \frac{1}{\alpha}\mathbf{j}_{n \times n} + \frac{1}{\alpha}\mathbf{W}\mathbf{j}_{m \times n} - \frac{1}{\alpha}\mathbf{j}_{n \times n} + \frac{1}{\alpha^2}\mathbf{j}_{n \times n}\mathbf{R}_f^{-1}\mathbf{j}_{n \times n} - \frac{1}{\alpha^2}\mathbf{W}\mathbf{j}_{m \times n}\mathbf{R}_f^{-1}\mathbf{j}_{n \times n} + \frac{1}{\alpha}\mathbf{j}_{n \times m}\mathbf{W}^t - \frac{1}{\alpha^2}\mathbf{j}_{n \times n}\mathbf{R}_f^{-1}\mathbf{j}_{n \times m}\mathbf{W}^t \right. \right. \\ &\quad \left. \left. + \frac{1}{\alpha^2}\mathbf{W}\mathbf{j}_{m \times n}\mathbf{R}_f^{-1}\mathbf{j}_{n \times m}\mathbf{W}^t \right) \mathbf{W}(\mathbf{W}^t\mathbf{W})^{-1}\mathbf{W}^t \right] \\ &= \text{Tr} \left[ \left( \mathbf{R}_f - \frac{2}{\alpha}\mathbf{j}_{n \times n} + \frac{1}{\alpha}\mathbf{W}\mathbf{j}_{m \times n} + \frac{1}{\alpha^2}\mathbf{j}_{n \times n}\mathbf{R}_f^{-1}\mathbf{j}_{n \times n} - \frac{1}{\alpha^2}\mathbf{W}\mathbf{j}_{m \times n}\mathbf{R}_f^{-1}\mathbf{j}_{n \times n} + \frac{1}{\alpha}\mathbf{j}_{n \times m}\mathbf{W}^t - \frac{1}{\alpha^2}\mathbf{j}_{n \times n}\mathbf{R}_f^{-1}\mathbf{j}_{n \times m}\mathbf{W}^t \right. \right. \\ &\quad \left. \left. + \frac{1}{\alpha^2}\mathbf{W}\mathbf{j}_{m \times n}\mathbf{R}_f^{-1}\mathbf{j}_{n \times m}\mathbf{W}^t \right) \mathbf{W}(\mathbf{W}^t\mathbf{W})^{-1}\mathbf{W}^t \right]. \end{aligned} \quad (\text{A3})$$

Rearranging the terms, we obtain

$$\begin{aligned} \text{Tr}[\mathbf{A}] = & \text{Tr} \left[ \mathbf{W}(\mathbf{W}^t \mathbf{W})^{-1} \mathbf{W}^t \mathbf{R}_f - \frac{2}{\alpha} \mathbf{W}(\mathbf{W}^t \mathbf{W})^{-1} \mathbf{W}^t \mathbf{j}_{n \times n} \right. \\ & + \frac{1}{\alpha^2} \mathbf{W}(\mathbf{W}^t \mathbf{W})^{-1} \mathbf{W}^t \mathbf{j}_{n \times n} \mathbf{R}_f^{-1} \mathbf{j}_{n \times n} + \frac{2}{\alpha} \mathbf{W} \mathbf{j}_{m \times n} \\ & - \frac{1}{\alpha^2} \mathbf{W} \mathbf{j}_{m \times n} \mathbf{R}_f^{-1} \mathbf{j}_{n \times n} - \frac{1}{\alpha^2} \mathbf{j}_{n \times n} \mathbf{R}_f^{-1} \mathbf{j}_{n \times m} \mathbf{W}^t \\ & \left. + \frac{1}{\alpha^2} \mathbf{W} \mathbf{j}_{m \times n} \mathbf{R}_f^{-1} \mathbf{j}_{n \times m} \mathbf{W}^t \right]. \end{aligned} \quad (\text{A4})$$

Substituting  $\text{Tr}[\mathbf{A}]$  into Eq. (A1), we obtain

$$\begin{aligned} \mathcal{J} = & \text{Tr} \left[ \mathbf{R}_f - \mathbf{W}(\mathbf{W}^t \mathbf{W})^{-1} \mathbf{W}^t \mathbf{R}_f \right. \\ & + \frac{1}{\alpha^2} \mathbf{W}(\mathbf{W}^t \mathbf{W})^{-1} \mathbf{W}^t \mathbf{j}_{n \times n} \mathbf{R}_f^{-1} \mathbf{j}_{n \times n} \\ & - \frac{1}{\alpha^2} \mathbf{W} \mathbf{j}_{m \times n} \mathbf{R}_f^{-1} \mathbf{j}_{n \times n} - \frac{1}{\alpha^2} \mathbf{j}_{n \times m} \mathbf{W}^t \mathbf{j}_{n \times n} \mathbf{R}_f^{-1} \\ & \left. + \frac{1}{\alpha^2} \mathbf{j}_{n \times m} \mathbf{W}^t \mathbf{W} \mathbf{j}_{m \times n} \mathbf{R}_f^{-1} + \mathbf{W} \mathbf{R}_z \mathbf{W}^t \right], \end{aligned} \quad (\text{A5})$$

which is the outer minimization problem described in Eq. (53). Once again, using the cyclic property of the trace of the product of matrices to make all products in the second parenthesis of Eq. (A6) of dimension  $m \times m$ ,

$$\begin{aligned} \mathcal{J} = & \text{Tr}[\mathbf{R}_f] - \text{Tr} \left[ (\mathbf{W}^t \mathbf{W})^{-1} \mathbf{W}^t \mathbf{R}_f \mathbf{W} \right. \\ & + \frac{1}{\alpha^2} (\mathbf{W}^t \mathbf{W})^{-1} \mathbf{W}^t \mathbf{j}_{n \times n} \mathbf{R}_f^{-1} \mathbf{j}_{n \times n} \mathbf{W} - \frac{2}{\alpha^2} \mathbf{j}_{m \times n} \mathbf{R}_f^{-1} \mathbf{j}_{n \times n} \mathbf{W} \\ & \left. + \frac{1}{\alpha^2} \mathbf{W}^t \mathbf{W} \mathbf{j}_{m \times n} \mathbf{R}_f^{-1} \mathbf{j}_{n \times m} + \mathbf{W}^t \mathbf{W} \mathbf{R}_z \right]. \end{aligned} \quad (\text{A6})$$

In order to obtain  $\mathbf{W}^*$ , we differentiate Eq. (A6) with respect to  $\mathbf{W}$  and set it to zero. We use the following standard identities [24] from matrix calculus to compute this derivative.

1. If  $\mathbf{B}$  and  $\mathbf{C}$  are symmetric matrices, then

$$\begin{aligned} \frac{d}{d\mathbf{X}} \text{Tr}[(\mathbf{X}^t \mathbf{C} \mathbf{X})^{-1} (\mathbf{X}^t \mathbf{B} \mathbf{X})] \\ = -2\mathbf{C} \mathbf{X} (\mathbf{X}^t \mathbf{C} \mathbf{X})^{-1} \mathbf{X}^t \mathbf{B} \mathbf{X} (\mathbf{X}^t \mathbf{C} \mathbf{X})^{-1} \\ + 2\mathbf{B} \mathbf{X} (\mathbf{X}^t \mathbf{C} \mathbf{X})^{-1}. \end{aligned} \quad (\text{A7})$$

2. If  $\mathbf{D}$  is a symmetric matrix, then

$$\frac{d}{d\mathbf{X}} \text{Tr}[\mathbf{X} \mathbf{D} \mathbf{X}^t] = 2\mathbf{X} \mathbf{D}. \quad (\text{A8})$$

Applying these two identities to differentiate Eq. (A6) with respect to  $\mathbf{W}$ , we obtain

$$\begin{aligned} \frac{\partial \mathcal{J}}{\partial \mathbf{W}} = & 2\mathbf{W}(\mathbf{W}^t \mathbf{W})^{-1} \mathbf{W}^t \mathbf{R}_f \mathbf{W}(\mathbf{W}^t \mathbf{W})^{-1} - 2\mathbf{R}_f \mathbf{W}(\mathbf{W}^t \mathbf{W})^{-1} \\ & - \frac{2}{\alpha^2} \mathbf{W}(\mathbf{W}^t \mathbf{W})^{-1} \mathbf{W}^t \mathbf{j}_{n \times n} \mathbf{R}_f^{-1} \mathbf{j}_{n \times n} \mathbf{W}(\mathbf{W}^t \mathbf{W})^{-1} \\ & + \frac{2}{\alpha^2} \mathbf{j}_{n \times n} \mathbf{R}_f^{-1} \mathbf{j}_{n \times n} \mathbf{W}(\mathbf{W}^t \mathbf{W})^{-1} - \frac{2}{\alpha^2} \mathbf{j}_{n \times n} \mathbf{R}_f^{-1} \mathbf{j}_{n \times m} \\ & + \frac{2}{\alpha^2} \mathbf{W} \mathbf{j}_{m \times n} \mathbf{R}_f^{-1} \mathbf{j}_{n \times m} + 2\mathbf{W} \mathbf{R}_z = 0. \end{aligned} \quad (\text{A9})$$

Note that Eq. (A9) is the equation we need to solve to obtain for the optimal reconstruction filter in terms of  $\mathbf{R}_f$  and  $\mathbf{R}_z$ .

## Appendix B: Simplification of Outer Minimization Problem

In this appendix, we show that solving for the solution to the inner energy constrained minimization problem (55) and the Wiener filter solution (54) is equivalent to solving the outer minimization problem in Eq. (A9). Substituting Eq. (55) into Eq. (54), we obtain

$$\begin{aligned} \mathbf{W} = & \left( \mathbf{R}_f - \frac{1}{\alpha} \mathbf{j}_{n \times n} + \frac{1}{\alpha} \mathbf{j}_{n \times m} \mathbf{W}^t \right) \mathbf{W}(\mathbf{W}^t \mathbf{W})^{-1} \\ & \times \left[ (\mathbf{W}^t \mathbf{W})^{-1} \mathbf{W}^t \left( \mathbf{R}_f - \frac{1}{\alpha} \mathbf{j}_{n \times n} + \frac{1}{\alpha} \mathbf{W} \mathbf{j}_{m \times n} \right) \mathbf{R}_f^{-1} \right. \\ & \left. \times \left( \mathbf{R}_f - \frac{1}{\alpha} \mathbf{j}_{n \times n} + \frac{1}{\alpha} \mathbf{j}_{n \times m} \mathbf{W}^t \right) \mathbf{W}(\mathbf{W}^t \mathbf{W})^{-1} + \mathbf{R}_z \right]^{-1} \end{aligned} \quad (\text{B1})$$

$$\begin{aligned} \Rightarrow & \mathbf{W} \left[ (\mathbf{W}^t \mathbf{W})^{-1} \mathbf{W}^t \left( \mathbf{R}_f - \frac{1}{\alpha} \mathbf{j}_{n \times n} + \frac{1}{\alpha} \mathbf{W} \mathbf{j}_{m \times n} \right) \mathbf{R}_f^{-1} \right. \\ & \times \left( \mathbf{R}_f - \frac{1}{\alpha} \mathbf{j}_{n \times n} + \frac{1}{\alpha} \mathbf{j}_{n \times m} \mathbf{W}^t \right) \mathbf{W}(\mathbf{W}^t \mathbf{W})^{-1} + \mathbf{R}_z \left. \right] \\ = & \left( \mathbf{R}_f - \frac{1}{\alpha} \mathbf{j}_{n \times n} + \frac{1}{\alpha} \mathbf{j}_{n \times m} \mathbf{W}^t \right) \mathbf{W}(\mathbf{W}^t \mathbf{W})^{-1}. \end{aligned} \quad (\text{B2})$$

Simplifying the terms, we obtain

$$\begin{aligned} \mathbf{W} \left[ \left( (\mathbf{W}^t \mathbf{W})^{-1} \mathbf{W}^t \mathbf{R}_f - \frac{1}{\alpha} (\mathbf{W}^t \mathbf{W})^{-1} \mathbf{W}^t \mathbf{j}_{n \times n} + \frac{1}{\alpha} \mathbf{j}_{m \times n} \right) \right. \\ \times \left( \mathbf{W}(\mathbf{W}^t \mathbf{W})^{-1} - \frac{1}{\alpha} \mathbf{R}_f^{-1} \mathbf{j}_{n \times n} \mathbf{W}(\mathbf{W}^t \mathbf{W})^{-1} \right. \\ \left. \left. + \frac{1}{\alpha} \mathbf{R}_f^{-1} \mathbf{j}_{n \times m} \right) + \mathbf{R}_z \right] \\ = \left( \mathbf{R}_f - \frac{1}{\alpha} \mathbf{j}_{n \times n} + \frac{1}{\alpha} \mathbf{j}_{n \times m} \mathbf{W}^t \right) \mathbf{W}(\mathbf{W}^t \mathbf{W})^{-1}. \end{aligned} \quad (\text{B3})$$

Bringing all the terms to one side yields

$$\begin{aligned}
0 = & \mathbf{W}(\mathbf{W}^t\mathbf{W})^{-1}\mathbf{W}^t\mathbf{R}_f\mathbf{W}(\mathbf{W}^t\mathbf{W})^{-1} \\
& - \frac{1}{\alpha}\mathbf{W}(\mathbf{W}^t\mathbf{W})^{-1}\mathbf{W}^t\mathbf{j}_{n \times n}\mathbf{W}(\mathbf{W}^t\mathbf{W})^{-1} \\
& + \frac{1}{\alpha}\mathbf{W}\mathbf{j}_{m \times n}\mathbf{W}(\mathbf{W}^t\mathbf{W})^{-1} \\
& - \frac{1}{\alpha}\mathbf{W}(\mathbf{W}^t\mathbf{W})^{-1}\mathbf{W}^t\mathbf{j}_{n \times n}\mathbf{W}(\mathbf{W}^t\mathbf{W})^{-1} \\
& + \frac{1}{\alpha^2}\mathbf{W}(\mathbf{W}^t\mathbf{W})^{-1}\mathbf{W}^t\mathbf{j}_{n \times n}\mathbf{R}_f^{-1}\mathbf{j}_{n \times n}\mathbf{W}(\mathbf{W}^t\mathbf{W})^{-1} \\
& - \frac{1}{\alpha^2}\mathbf{W}\mathbf{j}_{m \times n}\mathbf{R}_f^{-1}\mathbf{j}_{n \times n}\mathbf{W}(\mathbf{W}^t\mathbf{W})^{-1} \\
& + \frac{1}{\alpha}\mathbf{W}(\mathbf{W}^t\mathbf{W})^{-1}\mathbf{W}^t\mathbf{j}_{n \times m} \\
& - \frac{1}{\alpha^2}\mathbf{W}(\mathbf{W}^t\mathbf{W})^{-1}\mathbf{W}^t\mathbf{j}_{n \times n}\mathbf{R}_f^{-1}\mathbf{j}_{n \times m} \\
& + \frac{1}{\alpha^2}\mathbf{W}\mathbf{j}_{m \times n}\mathbf{R}_f^{-1}\mathbf{j}_{n \times m} + \mathbf{W}\mathbf{R}_z - \mathbf{R}_f\mathbf{W}(\mathbf{W}^t\mathbf{W})^{-1} \\
& + \frac{1}{\alpha}\mathbf{j}_{n \times n}\mathbf{W}(\mathbf{W}^t\mathbf{W})^{-1} - \frac{1}{\alpha}\mathbf{j}_{n \times m}. \tag{B4}
\end{aligned}$$

Recall that  $\alpha = \mathbf{j}_{1 \times n}\mathbf{R}_f^{-1}\mathbf{j}_{n \times 1}$ . Hence, the expression can be simplified as

$$\begin{aligned}
0 = & 2\mathbf{W}(\mathbf{W}^t\mathbf{W})^{-1}\mathbf{W}^t\mathbf{R}_f\mathbf{W}(\mathbf{W}^t\mathbf{W})^{-1} - 2\mathbf{R}_f\mathbf{W}(\mathbf{W}^t\mathbf{W})^{-1} \\
& - \frac{2}{\alpha^2}\mathbf{W}(\mathbf{W}^t\mathbf{W})^{-1}\mathbf{W}^t\mathbf{j}_{n \times n}\mathbf{R}_f^{-1}\mathbf{j}_{n \times n}\mathbf{W}(\mathbf{W}^t\mathbf{W})^{-1} \\
& + \frac{2}{\alpha^2}\mathbf{j}_{n \times n}\mathbf{R}_f^{-1}\mathbf{j}_{n \times n}\mathbf{W}(\mathbf{W}^t\mathbf{W})^{-1} - \frac{2}{\alpha^2}\mathbf{j}_{n \times n}\mathbf{R}_f^{-1}\mathbf{j}_{n \times m} \\
& + \frac{2}{\alpha^2}\mathbf{W}\mathbf{j}_{m \times n}\mathbf{R}_f^{-1}\mathbf{j}_{n \times m} + 2\mathbf{W}\mathbf{R}_z. \tag{B5}
\end{aligned}$$

Since Eq. (B5) is exactly same as (A9), solving Eqs. (54) and (55) jointly is equivalent to solving Eq. (A9).

### Appendix C: Optimality of Energy Conservation Design

To prove that the design procedure described in Subsection 4.C.1 is optimal, we substitute the proposed design choices into Eqs. (54) and (55). From Eqs. (54) and (55), we have

$$\begin{aligned}
\mathbf{H} = & (\mathbf{H}\mathbf{R}_f\mathbf{H}^t + \mathbf{R}_z)(\mathbf{H}\mathbf{R}_f^2\mathbf{H}^t)^{-1}\mathbf{H}\mathbf{R}_f \\
& \times \left( \mathbf{R}_f - \frac{1}{\alpha}\mathbf{j}_{n \times n} + \frac{1}{\alpha}\mathbf{R}_f\mathbf{H}^t(\mathbf{H}\mathbf{R}_f\mathbf{H}^t + \mathbf{R}_z)^{-1}\mathbf{j}_{m \times n} \right) \mathbf{R}_f^{-1}. \tag{C1}
\end{aligned}$$

Rewriting Eq. (C1) in terms of eigenvalue decomposition and SVDs of  $\mathbf{R}_f$ ,  $\mathbf{R}_z$ , and  $\mathbf{H}$ , we obtain

$$\begin{aligned}
\mathbf{U}\Sigma_{\mathbf{H}}\mathbf{V}^t = & (\mathbf{U}\Sigma_{\mathbf{H}}\mathbf{V}^t\mathbf{Q}_f\Lambda_f\mathbf{Q}_f^t\mathbf{V}\Sigma_{\mathbf{H}}^t\mathbf{U}^t + \mathbf{Q}_z\Lambda_z\mathbf{Q}_z^t) \\
& \times (\mathbf{U}\Sigma_{\mathbf{H}}\mathbf{V}^t\mathbf{Q}_f\Lambda_f^2\mathbf{Q}_f^t\mathbf{V}\Sigma_{\mathbf{H}}^t\mathbf{U}^t)^{-1} \\
& (\mathbf{U}\Sigma_{\mathbf{H}}\mathbf{V}^t\mathbf{Q}_f\Lambda_f\mathbf{Q}_f^t) \left( \mathbf{I} - \frac{1}{\alpha}\mathbf{j}_{n \times n}\mathbf{Q}_f\Lambda_f^{-1}\mathbf{Q}_f^t \right. \\
& + \frac{1}{\alpha}\mathbf{Q}_f\Lambda_f\mathbf{Q}_f^t\mathbf{V}\Sigma_{\mathbf{H}}^t\mathbf{U}^t(\mathbf{U}\Sigma_{\mathbf{H}}\mathbf{V}^t\mathbf{Q}_f\Lambda_f\mathbf{Q}_f^t\mathbf{V}\Sigma_{\mathbf{H}}^t\mathbf{U}^t \\
& \left. + \mathbf{Q}_z\Lambda_z\mathbf{Q}_z^t)^{-1}\mathbf{j}_{m \times n}\mathbf{Q}_f\Lambda_f^{-1}\mathbf{Q}_f^t \right). \tag{C2}
\end{aligned}$$

Substituting the design choices from Eq. (56),

$$\begin{aligned}
\Sigma_{\mathbf{H}} = & (\Sigma_{\mathbf{H}}\Lambda_{f,P}\Sigma_{\mathbf{H}}^t + \Lambda_z) \\
& \times (\Sigma_{\mathbf{H}}\Lambda_{f^2,P}\Sigma_{\mathbf{H}}^t)^{-1}\Sigma_{\mathbf{H}}\Lambda_{f,P} - \frac{1}{\alpha}(\Sigma_{\mathbf{H}}\Lambda_{f,P}\Sigma_{\mathbf{H}}^t + \Lambda_z) \\
& \times (\Sigma_{\mathbf{H}}\Lambda_{f^2,P}\Sigma_{\mathbf{H}}^t)^{-1}\Sigma_{\mathbf{H}}\Lambda_{f,P}\mathbf{a}\mathbf{a}^t\Lambda_{f^{-1},P} + \frac{1}{\alpha}\mathbf{b}\mathbf{a}^t\Lambda_{f^{-1},P}. \tag{C3}
\end{aligned}$$

Writing (C3) elementwise, the diagonal terms are

$$\sigma_{\mathbf{H}_i}^2\lambda_{fi}\mathbf{a}_i^2 - \sigma_{\mathbf{H}_i}\lambda_{fi}\mathbf{b}_i\mathbf{a}_i + \lambda_{zi}\mathbf{a}_i^2 - \lambda_{zi}\lambda_{fi} = 0, \tag{C4}$$

and the off-diagonal terms are

$$\sigma_{\mathbf{H}_i}^2\lambda_{fi}\mathbf{a}_i\mathbf{a}_j - \sigma_{\mathbf{H}_i}\lambda_{fi}\mathbf{b}_i\mathbf{a}_j + \lambda_{zi}\mathbf{a}_i\mathbf{a}_j = 0. \tag{C5}$$

By the large SNR approximation,  $\lambda_{zi} \rightarrow 0$ , we observe that (C4) and (C5) simplify to

$$\sigma_{\mathbf{H}_i} = \mathbf{b}_i/\mathbf{a}_i, \tag{C6}$$

i.e.,

$$\Sigma_{\mathbf{H}}\mathbf{a} = \mathbf{b}, \tag{C7}$$

which is the optimal design for the singular values of  $\mathbf{H}$  described in Subsection 4.C.1.

### References

1. J. Mait, "A history of imaging: revisiting the past to chart the future," *Opt. Photonics News* **17**, 22–27 (2006).
2. J. Mait, R. Athale, and J. van der Gracht, "Evolutionary paths in imaging and recent trends," *Opt. Express* **11**, 2093–2101 (2003).
3. T. Cathey and E. Dowski, "New paradigm for imaging systems," *Appl. Opt.* **41**, 6080–6092 (2002).
4. J. Tanida, T. Kumagai, K. Yamada, S. Miyatake, K. Ishida, T. Morimoto, N. Kondou, D. Miyazaki, and Y. Ichioka, "Thin observation module by bound optics TOMBO: concept and experimental verification," *Appl. Opt.* **40**, 1806 (2001).
5. F. Russell and J. Goodman, "Nonredundant arrays and post-detection processing for aberration compensation in incoherent imaging," *J. Opt. Soc. Am.* **61**, 182–191 (1971).
6. J. Duparré, P. Schreiber, P. Dannberg, T. Scharf, P. Pelli, R. Völkel, H. Herzig, and A. Bräuer, "Artificial compound eyes—different concepts and their application to ultraflat

- image acquisition sensors,” *Proc. SPIE* **5346**, 89–100 (2004).
7. E. Dowski and T. Cathey, “Extended depth of field through wave-front coding,” *Appl. Opt.* **34**, 1859–1866 (1995).
  8. M. Christensen, M. Haney, D. Rajan, S. Wood, and S. Douglas, “Panoptes: A thin agile multi-resolution imaging sensor,” presented at Government Microcircuit Applications and Critical Technology Conference (GOMACTech-05), 4–7 April 2005.
  9. M. Christensen, V. Bhakta, D. Rajan, T. Mirani, S. Douglas, S. Wood, and M. Haney, “Adaptive flat multiresolution multiplexed computational imaging architecture utilizing micro-mirror arrays to steer subimager fields of view,” *Appl. Opt.* **45**, 2884–2892 (2006).
  10. T. Mirani, M. Christensen, S. Douglas, D. Rajan, and S. Wood, “Optimal co-design of computational imaging systems,” in *IEEE International Conference on Acoustics, Speech, and Signal Processing, 2005. Proceedings (ICASSP '05)* (IEEE, 2005). Vol. **2**, pp. 597–600.
  11. A. Geoffrion, “Generalized benders decomposition,” *J. Optim. Theory Appl.* **10**, 237–260 (1972).
  12. S. Boyd and L. Vandenberghe, *Convex Optimization* (Cambridge U. Press, 2003).
  13. D. Luenberger, *Linear and Non-Linear Programming*, 2nd ed. (Springer, 2004).
  14. K. Diamantaras and S. Kung, *Principal Component Neural Networks: Theory and Applications* (Wiley, 1996).
  15. G. Strang, *Introduction to Linear Algebra*, 3rd ed. (Wellesley-Cambridge Press, 2003).
  16. G. Golub and C. Loan, *Matrix Computations*, 3rd ed. (Johns Hopkins U. Press, 1996).
  17. H. Andrews and B. Hunt, *Digital Image Restoration* (Prentice-Hall, 1977).
  18. R. Gonzalez and R. Woods, *Digital Image Processing*, 2nd ed. (Prentice Hall, 2002).
  19. P. K. Baheti and M. A. Neifeld, “Feature-specific structured imaging,” *Appl. Opt.* **45**, 7382–7391 (2006).
  20. A. Geoffrion, “Elements of large-scale mathematical programming,” *Manage. Sci.* **16**, 652–691 (1970).
  21. J. A. O’Sullivan, “Alternating minimization algorithms: from Blahut–Arimoto to expectation-maximization,” in *Codes, Curves, and Signals: Common Threads in Communications*, A. Vardy, ed. (Springer, 1998), pp. 173–192.
  22. J. Goodman, *Introduction to Fourier Optics*, 2nd ed. (McGraw-Hill, 1996).
  23. H. Faraji and W. James MacLean, “CCD noise removal in digital images,” *IEEE Trans. Image Process.* **15**, (2006).
  24. M. Brookes, *The Matrix Reference Manual* (Imperial College, 2005), <http://www.ee.ic.ac.uk/hp/staff/dmb/matrix/intro.html#Intro>.



# Queries

1. Applied Optics does not use bottom of the page style footnotes. Also, displayed this equation for readability.